
KERJEPAs: KERNEL DISCREPANCIES FOR EUCLIDEAN SELF-SUPERVISED LEARNING

Eric Zimmermann¹, Harley Wiltzer^{2,3}, Justin Szeto^{2,3}, David Alvarez-Melis¹, and Lester Mackey¹

¹Microsoft Research, Cambridge, MA United States

²Mila-Québec AI Institute, Montreal, Canada

³McGill University, Montreal, Canada

ABSTRACT

Recent breakthroughs in self-supervised Joint-Embedding Predictive Architectures (JEPAs) have established that regularizing Euclidean representations toward isotropic Gaussian priors yields provable gains in training stability and downstream generalization. We introduce a new, flexible family of KerJEPAs, self-supervised learning algorithms with kernel-based regularizers. One instance of this family corresponds to the recently-introduced LeJEPA Epps-Pulley regularizer which approximates a sliced maximum mean discrepancy (MMD) with a Gaussian prior and Gaussian kernel. By expanding the class of viable kernels and priors and computing the closed-form high-dimensional limit of sliced MMDs, we develop alternative KerJEPAs with a number of favorable properties including improved training stability and design flexibility.

1 Introduction

Self-supervised learning (SSL) methods aim to learn useful, general representations from unlabeled data by learning the underlying structure of the data itself. The promise of these methods is that the representations serve as strong features for arbitrary downstream tasks, enabling the construction of foundation models. In this work, we introduce and investigate a general framework for SSL on visual data which greatly generalizes the space of downstream tasks that can be accommodated, allowing practitioners to make informed algorithm design decisions.

A common approach to SSL, particularly in visual domains, is to project data points (say, images) to various *views* (say, random crops or rotations) and learn embeddings that map views of similar images to similar embeddings. A pitfall of such a framework is that it admits a trivial, pathological solution by mapping all inputs to the same embedding. To mitigate this issue, *regularization* is crucial: by regularizing the distribution of the learned embeddings to a fixed, user-designed *prior* distribution, representation collapse is avoidable. However, regularization of such high-dimensional distributions remains a sincere challenge, both in principle and in practice.

Historically, SSL methods have largely constrained embeddings to a hypersphere, which was found to stabilize training and induce bounded gradients and regularizers. More recently, there has been increasing interest in moving off the hypersphere, towards learning *Euclidean* representations [3, 4]. Particularly, the recent LeJEPA algorithm [3] argued that an *isotropic Gaussian* distribution over embeddings is optimal for downstream regression and classification tasks with weight decay—notably, this is not achievable with hyperspherical representations. In order to induce such a distribution over representations, they introduce a novel regularizer that regularizes randomly sampled univariate projections of the embedding distributions to univariate isotropic Gaussians. This approach is principled and achieves state-of-the-art performance on downstream image regression and classification tasks.

Despite these successes, this reliance on stochastic projections introduces a fundamental tension between estimation variance and computational cost. While sliced matching is guaranteed to converge, the finite approximation of the integral over the sphere introduces gradient noise that scales with the embedding dimension. To maintain training stability and convergence rates in high-dimensional regimes, the number of projections must be increased, which eventually undermines the linear computational scaling that slicing aims to provide. Current sliced approaches specialize to Gaussian priors with a fixed Gaussian kernel, motivated by a result that isotropically-Gaussian-distributed features are

optimal for downstream ℓ_2 -regularized tasks. Unfortunately, this ignores the distribution shift between the regularized features and those used for transfer in SSL pipelines. This rigidity precludes the exploration of alternative regularizers, non-Gaussian priors, and heavy-tailed kernels which may offer superior geometric properties for downstream tasks.

In this work, we identify a common algorithmic structure for Euclidean regularization in SSL, generalizing the individual components of LeJEPa. Particularly, we devise a framework that accommodates myriad downstream objectives beyond ℓ_2 -regularized varieties, and unveils a *family* of discrepancies that can achieve the requisite regularization. Notably, our framework allows us to deeply study the computational and statistical tradeoffs in high-dimensional distributional regularization for SSL. Through empirical analysis, we derive guidelines for how to navigate these tradeoffs when scaling the minibatch and embedding dimension.

2 Related Work

While the broader goal of SSL is to learn augmentation-invariant representations, specific methods diverge in how they prevent the trivial collapse mentioned in the introduction. *Contrastive* methods, such as SimCLR [12] and MoCo [22], avoid collapse by explicitly pushing apart the representations of distinct samples (negative pairs) while attracting positive pairs. *Non-contrastive* methods eliminate the need for negative pairs, relying instead on architectural asymmetries or statistical constraints. For instance, BYOL [21] utilizes stop-gradient mechanisms, while Barlow Twins [39], VICReg [4], and HSIC-SSL [27] impose variance-preservation, de-correlation, or moment-matching objectives on the embedding dimensions.

Crucial to all these frameworks is the design of data augmentations, which implicitly defines which features are learned. Techniques such as cropping, color jittering, and Gaussian blur encourage the network to discard low-level visual statistics [29], while advanced strategies like multicrop [11] enforce consistency across varying spatial scales. Equally important is the standard backbone-projector architectures. Empirical success in SSL heavily relies on the guillotine regularization: discarding the non-linear projection head after pretraining and utilizing only the backbone features for downstream tasks [10]. This structural decoupling implies that the training objective, which is applied to the projections, does not directly constrain the geometry of the representations used for transfer. This misalignment draws attention to the benefits of selecting a particular geometry throughout training, which we explicitly address in our work.

A dominant paradigm in SSL involves normalizing embeddings to the unit hypersphere, effectively fixing the scale of representation to focus learning entirely on angular relationships. This geometric constraint naturally leads to objectives that encourage the uniform distribution of features over the sphere, thereby maximizing the information entropy of the induced distribution [37]. More sophisticated distribution matching has been approached through optimal transport, specifically using the Spherical Sliced Wasserstein (SSW) distance [8], which leverages random projections to align the empirical distribution of embeddings with a uniform target. Similarly, kernel-based methods have been applied via Hilbert-Schmidt Independence Criterion [27]. These works demonstrated the utility of both slicing and kernel discrepancies, providing a foundation for their extension into other geometries.

The recent shift toward isotropic Gaussian targets in Euclidean space, exemplified by LeJEPa [3] which builds on VICReg [4, 34], bridges SSL with kernel-based methods, without explicit normalization. Although LeJEPa formulates its regularizer (SIGReg) via the *Epps-Pulley test* [15] on random projections, recent analyses establish that this is effectively equivalent to minimizing the Sliced Maximum Mean Discrepancy (MMD) between the embeddings and the target Gaussian [13, 35]. Based on this categorization, there is a plethora of novel discrepancies and kernel methods that can be explored in a similar setting [17, 25, 28], which we investigate in the sequel.

3 Matching Distributions with Kernel Discrepancies

In the following section, we introduce concepts and methods for matching empirical distributions to target distributions and explicitly connect a special case of Maximum Mean Discrepancy with the Epps-Pulley test statistic used by LeJEPa. We leverage these tools as a means of replacing SIGReg in the LeJEPa framework with alternative measures between distributions such as *Stein’s method*. Overall, we draw attention to how different methods can be approximated and what the role of a known prior induces in terms of required samples.

3.1 Kernels, Reproducing Kernel Hilbert Spaces, and Distribution Comparison

Kernel methods provide a powerful framework for comparing probability distributions by embedding them into a *Reproducing Kernel Hilbert Space* (RKHS) [2]. Let $k : \mathbb{R}^d \times \mathbb{R}^d \rightarrow \mathbb{R}$ be a positive definite kernel with associated RKHS \mathcal{H} . The kernel defines a feature map $\phi : \mathbb{R}^d \rightarrow \mathcal{H}$ such that $k(x, x') = \langle \phi(x), \phi(x') \rangle_{\mathcal{H}}$. For any probability

distribution P on \mathbb{R}^d , its *kernel mean embedding* is defined as

$$\mu_P = \mathbb{E}_{X \sim P}[k(X, \cdot)] = \mathbb{E}_{X \sim P}[\phi(X)] \in \mathcal{H}. \quad (1)$$

This embedding maps a distribution into the RKHS, allowing us to measure distances between distributions via their embeddings. If the kernel k is *characteristic*, this mapping is injective: $\mu_P = \mu_Q$ if and only if $P = Q$ [35]. This property ensures that kernel-based discrepancies capture full distributional differences, not merely differences in low-order moments.

Often, one employs a continuous, shift-invariant kernel $k(x, y) = k(x - y)$, which, by *Bochner's Theorem* [33], admits a Fourier representation on non-negative Borel measures with a *spectral density* ρ_k defined as

$$k(x - y) = \int_{\mathbb{R}^d} \exp(i\omega^\top(x - y))\rho_k(\omega)d\omega. \quad (2)$$

An instance of this shift-invariant kernel is the *Gaussian Kernel*,

$$k_{\text{gsn}}(x, y) = \exp(-\gamma\|x - y\|_2^2), \quad \rho_{\text{gsn}}(\omega) = \frac{1}{(4\pi\gamma)^{d/2}} \exp\left(-\frac{1}{4\gamma}\|\omega\|_2^2\right), \quad (3)$$

where $\gamma > 0$ is a bandwidth parameter. The choice of kernel and bandwidth is critical, as its selection controls sensitivity to local versus global structure. Small γ emphasizes fine-scale differences, while large γ smooths over local variations. Bandwidth selection therefore directly impacts the ability to accurately estimate the population distribution and detect deviations from the target prior. We provide additional examples of shift-invariant kernels in App. A.

3.2 Maximum Mean Discrepancy

The *Maximum Mean Discrepancy* (MMD) is an RKHS distance measure between probability distributions P and Q defined via kernel mean embeddings from each distribution. For a kernel k associated with RKHS \mathcal{H} , it is defined as

$$\text{MMD}_k(P, Q) = \|\mu_P - \mu_Q\|_{\mathcal{H}}. \quad (4)$$

Equivalently, the square of this metric has the following useful form:

$$\text{MMD}_k^2(P, Q) = \mathbb{E}_{X, X' \sim P}[k(X, X')] + \mathbb{E}_{Y, Y' \sim Q}[k(Y, Y')] - 2\mathbb{E}_{X \sim P, Y \sim Q}[k(X, Y)]. \quad (5)$$

It is also possible to define the MMD for general shift invariant kernel under Bochner's theorem as

$$\text{MMD}_k^2(P, Q) = \int_{\mathbb{R}^d} |\phi_P(\omega) - \phi_Q(\omega)|^2 \rho_k(\omega) d\omega, \quad (6)$$

where $\phi(\omega)$ is the *Characteristic Function* (CF) for both P and Q and ρ_k is the spectral density of k (cf. (2)). In §Sec. 3.2.1, we will use the representation (6) to connect MMD to the Epps-Pulley hypothesis test recommended in LeJEPA [3].

3.2.1 Epps-Pulley via Maximum Mean Discrepancy

LeJEPA selects the *Epps-Pulley* (EP) [15] test as the isotropic Gaussian regularizer of choice. We note that the exact EP test statistic is a scaled kernel MMD [13, 20, 35], where LeJEPA approximates the test statistic to avoid the usual quadratic cost of MMD. We directly characterize this relationship below.

The Epps-Pulley test is closely related to the function $\text{EP} : \mathcal{P}(\mathbb{R}) \rightarrow \mathbb{R}_+$ given by

$$\text{EP}(P) = \int_{\mathbb{R}} |\phi_P(\omega) - \phi_N(\omega)|^2 \rho(\omega) d\omega, \quad (7)$$

where $N = \mathcal{N}(0, \sigma^2)$, and where ϕ_P denotes the CF corresponding to the probability measure P , and ρ is a weighting function. In LeJEPA, we take ρ to be the spectral density of a Gaussian kernel with bandwidth $\gamma > 0$ (cf. (18)). Under this choice, by comparison to (6), we see that EP is simply a particular MMD, as we state below:

Proposition 1 $\text{EP}(P) = \text{MMD}_{k_{\text{gsn}}}^2(P, \mathcal{N}(0, \sigma^2))$.

The *Epps-Pulley test* $\widehat{\text{EP}}$ is a statistical test for determining whether a population is likely to be normally-distributed, which is used to derive the regularizer in LeJEPa. The test is defined as follows,

$$\widehat{\text{EP}}_n(P) = n\text{EP}(\widehat{P}_n), \quad \widehat{P}_n = \frac{1}{n} \sum_{i=1}^n \delta_{X_i}, \quad X_i \stackrel{\text{iid}}{\sim} P. \quad (8)$$

This is a statistic that can be estimated by simply sampling from P when its CF is unknown. In LeJEPa, the integral (8) (cf. (7)) is approximated via quadrature—this introduces additional hyperparameters, such as the quadrature rule and the number of knots, but provides sufficient approximation in practice [3].

Moreover, we note that this test is a consistent estimator for EP, as shown in the following result:

Proposition 2 ([3], Theorem 6) $\left| \mathbb{E}[n^{-1}\widehat{\text{EP}}_n(P)] - \text{EP}(P) \right| \leq O(1/n)$.

Thus, by Proposition Thm. 1, we have the following corollary,

Corollary 3 ([3], Theorem 6) $\left| \mathbb{E}[n^{-1}\widehat{\text{EP}}_n(P)] - \text{MMD}_{k_{\text{gsn}}}^2(P, \mathcal{N}(0, \sigma^2)) \right| \leq O(1/n)$.

Note that these statistical tests are limited to *univariate* variables, while in practice, the aim is to regularize distributions over high-dimensional latents. Ultimately, these tests can be *lifted* to distributions over \mathbb{R}^d with a technique known as *slicing*; this will be discussed in §Sec. 3.4. Foreshadowing, by drawing the connection between the Epps-Pulley test and MMD, one might consider alternatively designing regularizers directly via MMD, which admits unbiased sample-based estimators for multivariate distributions and dimension-free sample complexity—this is shown explicitly in Appendix App. C; which is equivalent to the multivariate extension called the Baringhaus-Henze-Epps-Pulley (BHEP) test [5].

3.3 Kernel Stein Discrepancy

One valuable feature of the Gaussian MMD (and Epps-Pulley) test is that the Gaussian kernel has a known integral under $Q = \mathcal{N}(0, \sigma^2)$ so that one can measure distance to a Gaussian directly without requiring a sample approximation of Q . We next introduce a second kernel that has this property both for Gaussian Q and for a much broader family of alternative prior distributions, the *Stein kernel*. The Kernel Stein Discrepancy (KSD) [13, 19, 25, 28] eliminates the need for the normalization constant entirely. By leveraging the Langevin Stein operator [18], KSD depends only on the score function $s_Q(x) = \nabla_x \log Q(x)$ of the target¹ Q . This makes KSD particularly advantageous for high-dimensional self-supervised learning with a known target prior, as it allows us to match the target geometry exactly through closed-form gradients without the variance induced by target sampling.

The foundation of KSD lies in the Stein operator A_Q , which acts on a vector-valued test function $f : \mathbb{R}^d \rightarrow \mathbb{R}^d$ via the identity $(A_Q f)(x) = s_Q(x)^\top f(x) + \nabla_x \cdot f(x)$. Under mild regularity conditions, the expectation of this operator under the target distribution vanishes, meaning $\mathbb{E}_{X \sim Q}[(A_Q f)(X)] = 0$. Consequently, for any distribution $P \neq Q$, the magnitude of this expectation serves as a discrepancy measure. Squaring the discrepancy allows us to apply the kernel reproducing property, recovering a closed-form expectation under P :

$$\text{KSD}^2(P, Q) = \mathbb{E}_{X, X' \sim P}[k_{\text{stein}}(X, X')], \quad (9)$$

where the Stein kernel k_{stein} is defined by applying the Stein operator to both arguments of a base kernel k :

$$k_{\text{stein}}(x, y) = s_Q(x)^\top k(x, y) s_Q(y) + s_Q(x)^\top \nabla_y k(x, y) + \nabla_x k(x, y)^\top s_Q(y) + \text{tr}(\nabla_x \nabla_y^\top k(x, y)). \quad (10)$$

Theoretically, this discrepancy can be viewed as a special MMD in which the target-dependent terms vanish due to Stein’s identity, leaving a measure that depends solely on the interaction of samples from P through the geometry of Q [6]. This interaction characterizes the discrepancy between the sample distribution and the target. Furthermore, for specific classes of kernels, and dimension, KSD metrizes weak convergence. This property is vital for self-supervised learning, as it ensures that a sequence of distributions minimizing the loss converges to the target distribution in law, preventing the representation collapse often observed when minimizing simpler moment-matching objectives.

Certain studies have observed that the KSD hypothesis test with a Gaussian base kernel forms a more powerful normality test than the MMD-based BHEP test [13]. Additionally, it has been shown that the KSD with an IMQ kernel offers even greater statistical testing power than its Gaussian counterpart, particularly in detecting deviations in the tails [19]. Thus, this is strong motivation for incorporating KSD regularizers with various kernels into our SSL methods.

¹Here, $\log Q$ refers to the log-density of an absolutely continuous distribution Q .

3.3.1 Spectral Representation of the Kernel Stein Discrepancy

The KSD with shift-invariant kernels may also be written in terms of the spectral representation via Bochner’s theorem, yielding an alternative avenue for estimation:

Proposition 4 For a probability distribution Q , let s_Q denote its score $\nabla \log Q$. For any shift-invariant kernel k ,

$$\text{KSD}_k^2(P, Q) = \int_{\mathbb{R}^d} \left\| \mathbb{E}_{X \sim P} [(s_Q(X) + i\omega) \exp(i\omega^\top X)] \right\|^2 \rho_k(\omega) d\omega,$$

where ρ_k is the spectral density of the kernel k .

[Proof]

Specializing to the Gaussian prior as in LeJEPA with the Epps-Pulley regularizer, the following emerges immediately as a special case of Proposition Thm. 4.

Corollary 5 For any shift-invariant kernel k , it holds that

$$\text{KSD}_k^2(P, \mathcal{N}(0, \sigma^2 I_d)) = \int_{\mathbb{R}^d} \left\| \omega \phi_P(\omega) + \frac{1}{\sigma^2} \nabla_\omega \phi_P(\omega) \right\|^2 \rho_k(\omega) d\omega,$$

where ϕ_P is the CF of the distribution P .

[Proof]

One can readily construct a V -estimator based on the expressions of the squared KSD of Proposition Thm. 4 and Corollary Thm. 5 by substituting P with an empirical distribution \hat{P}_n sampled from P ; such estimators incur a bias of $O(1/n)$ for bounded kernels k .

This spectral formulation enables us to leverage the same computational tricks as LeJEPA to minimize sample complexity via quadrature approximation, for example, using Gauss-Hermite polynomials combined with the Gaussian kernel. We also note that this form can be approximated efficiently using random features [23] as well.

3.4 Sliced Integral Probability Metrics

Integral Probability Metrics (IPMs) have analytical properties for reasoning about the similarity of complex probability distributions, however, they often present serious difficulties when it comes to estimating distances between multivariate variables from samples. For instance, while univariate p -Wasserstein distances are fairly simple to estimate due to their special characterization via metrics on CDFs [36], once $d > 1$, Wasserstein distances no longer have a closed-form solution and need to be estimated, and sample-based estimators of the Wasserstein metrics are known to be *biased* [7]. Issues such as this one motivated the concept of *sliced Wasserstein distances* [9, 31], which averages the Wasserstein distance over all univariate projections (that is, over the uniform distribution $\mathcal{U}(\mathbb{S}^{d-1})$ on \mathbb{S}^{d-1}) of the distributions being compared; for any such projection, an unbiased estimator of the Wasserstein distance can be computed efficiently.

More generally, the concept of slicing can alleviate several computational challenges arising from the sample-based estimation of multivariate random variable discrepancies. Explicitly, such approaches leverage the celebrated *Cramér-Wold* theorem, stated below.

Theorem 6 (Cramér-Wold) Let $X \sim P$ and $Y \sim Q$ denote random vectors taking values in \mathbb{R}^d . Then

$$X \stackrel{\text{law}}{=} Y \iff \xi^\top X \stackrel{\text{law}}{=} \xi^\top Y, \quad \forall \xi \in \mathbb{S}^{d-1}.$$

This theorem demonstrates that it is sufficient to compare random variables by one-dimensional projections, which motivates the concept of sliced divergences.

Definition 1 (Sliced divergence) Let $\mathcal{P}(\mathcal{X})$ denote the space of probability measures over a set \mathcal{X} . Any metric $d : \mathcal{P}(\mathbb{R}) \times \mathcal{P}(\mathbb{R}) \rightarrow \mathbb{R}_+$ can be lifted to a divergence on $\mathcal{P}(\mathbb{R}^d)$ through the slice operator S defined by:

$$(Sd)(P, Q) := \mathbb{E}_{\xi \sim \mathcal{U}(\mathbb{S}^{d-1})} [d(\xi_\#^\top P, \xi_\#^\top Q)].$$

As an immediate note, whenever the base metric d admits an unbiased sample estimator, Sd does as well: simply sample several directions ξ independently and uniformly on \mathbb{S}^{d-1} , and then compute the unbiased estimates $d(\xi_\#^\top P, \xi_\#^\top Q)$. For a base divergence d with sample complexity $\beta(d, n)$ for n samples drawn from the probability distributions under comparison, this Monte-Carlo sliced distance estimator has sample complexity bounded [30, Corollary S4] by

$$\beta(d, n) + \frac{1}{\sqrt{m}} \sqrt{\mathbb{E} \left[\text{Var} \left\{ \hat{d}(\xi_\#^\top P) \right\} \right]} \quad (11)$$

where m is the number of random directions sampled, and $\widehat{d}(\xi_{\#}^{\top} P)$ is the empirical estimate of $d(\xi_{\#}^{\top} P, \xi_{\#}^{\top} Q)$ from n samples of P . Depending on the instantiations of d and P , this sample complexity can be considerably less desirable, but it is generally difficult to characterize. Indeed, LeJEPa also finds that their sliced EP error bound grows with dimension [3, Theorem 5].

However, certain metrics like the MMD admit unbiased sample-based estimators, and incur *dimension-free* sample complexity: that is, the number of samples required to estimate a distribution to within a given tolerance with respect to the MMD is independent of d , so the MMD circumvents the curse of dimensionality. Thus, the question remains: what is the impact of slicing for such metrics?

Even for metrics on $\mathcal{P}(\mathbb{R}^d)$ that admit unbiased estimators for multivariate variables, slicing may still provide computational benefits in certain cases. The MMD family of metrics [20] can be estimated by computing pairwise kernel evaluations across samples from P, Q , however, this scales quadratically in the number of samples, which may be practically infeasible. Alternatively, one might compute these metrics in the Fourier domain (e.g. (6)), but computing the resulting integral suffers from the curse of dimensionality in general. With slicing, a base MMD metric can be evaluated in the Fourier domain by simply approximating an integral over \mathbb{R} , without requiring pairwise kernel evaluations; this is precisely the approach of LeJEPa [3]. Using stochastic gradient optimization, independently resampling directions ξ on each minibatch update yields a distribution matching scheme that does not suffer from the curse of dimensionality [3].

3.5 Tradeoffs with Sliced Metrics

In the previous section, we saw that slicing multivariate metrics enables efficient (approximately-)unbiased estimators of high-dimensional probability metrics. However, the computational efficiency of the sliced procedure leading up to the SIGReg regularizer come with certain costs, most notably:

1. **Approximation bias.** The (sliced) Epps-Pulley integrals must be approximated e.g. via quadrature;
2. **Increased variance.** In practice, expectations over slice directions are estimated by Monte Carlo (e.g., by sampling uniformly random directions) which incurs additional variance.

Fortunately, these costs can be eliminated with computation, as we will see in this section. First, we establish that SIGReg regularization is equivalent to MMD regularization with a particular kernel.

Theorem 7 Let $\text{SIGReg} : \mathcal{P}(\mathbb{R}^d) \rightarrow \mathbb{R}_+$ denote the SIGReg regularizer [3]; that is,

$$\text{SIGReg}(P) := \mathbb{E}_{\xi \sim \mathcal{U}(\mathbb{S}^{d-1})} [n^{-1} \text{EP}(\xi_{\#}^{\top} P)].$$

It holds that SIGReg is equivalent to a particular MMD,

$$\text{SIGReg}(P) = \text{MMD}_{\kappa_d}^2(P, \mathcal{N}(0, \sigma^2 I_d)), \quad \kappa_d(x, y) := {}_1F_1\left(\frac{1}{2}; \frac{d}{2}; -\gamma \|x - y\|_2^2\right),$$

where ${}_1F_1$ is the Kummer Confluent Hypergeometric function, and MMD_k denotes the MMD under the kernel k . Particularly, κ_d has polynomially decaying tails (as opposed to exponentially decaying tails like k_{gsn}). [\[Proof\]](#)

Theorem Thm. 7 sheds light on the induced *geometry* imposed on the latent embeddings by the slicing operation. Notably, it imposes a *heavy tailed* similarity measure between latent embeddings, as opposed to commonly used subgaussian-tailed kernels such as k_{gsn} . Additionally, the equivalent kernel induced by slicing is *dimension-dependent*: as we scale the dimension, the slicing operation effectively decreases the *bandwidth* of the resulting kernel. These insights will serve as critical considerations when designing and interpreting alternative regularization schemes downstream.

We now shift our attention back to the two issues highlighted above, in light of Theorem Thm. 7. First, we address the variance induced by slicing by proving a SIGReg estimator that avoids slicing altogether, at the cost of computing pairwise kernel evaluations.

Theorem 8 Let $P \in \mathcal{P}(\mathbb{R}^d)$, and let $\widehat{P}_n := (X_i)_{i=1}^n \stackrel{\text{iid}}{\sim} P$. Define the estimator $\widehat{\text{MMD-Gauss}}_{\kappa_d} : \mathbb{R}^{d \times n} \rightarrow \mathbb{R}_+$ according to

$$\widehat{\text{MMD-Gauss}}_{\kappa_d}^2(\widehat{P}_n) := \frac{1}{n(n-1)} \sum_{i=1}^n \sum_{j \neq i} \kappa_d(X_i, X_j) - \frac{2}{n\sqrt{1+2\gamma\sigma^2}} \sum_{i=1}^n {}_1F_1\left(\frac{1}{2}; \frac{d}{2}; -\frac{\gamma}{1+2\gamma\sigma^2} \|X_i\|_2^2\right) + C \tag{12}$$

for some constant C independent of P . Then $\widehat{\text{MMD-Gauss}}_{\kappa_d}^2(\widehat{P}_n)$ is an unbiased estimate of $\text{SIGReg}(P)$, and $|\mathbb{E}[\widehat{\text{MMD-Gauss}}_{\kappa_d}^2(\widehat{P}_n) - \text{SIGReg}(\widehat{P}_n)]| \leq O(1/n)$. [\[Proof\]](#)

The estimator of Theorem Thm. 8 presents interesting tradeoffs relative to the sliced Epps-Pulley estimator of LeJEPa [3]. Both estimators require samples \widehat{P}_n from P . The tradeoffs lie in which additional random samples are required, as well as computational efficiency. Notably, the $\widehat{\text{MMD-Gauss}}_{\kappa_d}^2$ estimator avoids Monte-Carlo sampling slice directions by effectively computing the expectation over directions in closed form—this is what brings us from the simple k_{gsn} kernel to κ_d and ${}_1F_1$ evaluations. Moreover, in principle, $\widehat{\text{MMD-Gauss}}_{\kappa_d}^2$ is *unbiased*, unlike the implementation of LeJEPa which requires approximating a Fourier integral via quadrature methods. However, these advantages come at a computational cost, which we discuss next. In transitioning from sampling directions and evaluating univariate MMDs (e.g., Epps-Pulley tests), we must perform pairwise kernel evaluations, costing $O(n^2)$ computation as opposed to the $O(n)$ complexity of LeJEPa. Moreover, computing ${}_1F_1$ is generally intractable, and expensive to approximate—thus, this incurs additional computational expense, and indeed as a result $\widehat{\text{MMD-Gauss}}_{\kappa_d}^2$ must be biased in practice. We do note, however, that in the setting of large embedding dimension, ${}_1F_1(1/2, d/2, \cdot)$ is well-approximated [24] by the *inverse multiquadric kernel* $k_{\text{imq}}^{\alpha, \beta}(x, y) = (1 + \alpha\|x - y\|_2^2)^{-\beta}$, that is

$${}_1F_1\left(\frac{1}{2}; \frac{d}{2}; -c\right) - \frac{1}{\sqrt{1 + \frac{4}{2d-3}c}} \xrightarrow{d \uparrow \infty} 0. \quad (13)$$

Note that, with $c := \gamma\|x - y\|_2^2$ in (13), we see that ${}_1F_1(1/2; d/2; \gamma\|x - y\|_2^2)$ can be approximated by the simpler $k_{\text{imq}}^{\alpha, \beta}(x, y)$ for $\alpha = 4\gamma(2d - 3)^{-1}$ and $\beta = 1/2$ when d is large. The work of [24] found that convergence is effectively reached for $d \geq 20$, making this practical for large-scale applications.

Altogether, both practical implementations of $\widehat{\text{MMD-Gauss}}_{\kappa_d}^2$ and that of LeJEPa induce a small bias, and the former expends quadratic compute to eliminate the variance of Monte-Carlo slicing. With large distributed training setups, we argue that it is worth investigating which side of this tradeoff is favorable, or identifying situations when one approach may be preferred over the other. That said, it is important to note that **slicing divergences is not necessary or sufficient for breaking the curse of dimensionality**. We showed in this section that equivalent regularizers can be derived (and indeed, generalized) without slicing at all.

3.6 Sliced Kernel Stein Discrepancy

We now derive the closed-form estimator for the Sliced Kernel Stein Discrepancy (SKSD) using the analytic Cramér-Wold approximation. Similar to the MMD derivation in Appendix App. E, we define the Sliced KSD as the expectation of the KSD over one-dimensional projected marginals, where henceforth we write $\mathcal{U} = \mathcal{U}(\mathbb{S}^{d-1})$:

$$\text{SKSD}^2(P, Q) = \int_{\mathbb{S}^{d-1}} \text{KSD}^2(\xi_{\#}P, \xi_{\#}Q) d\mathcal{U}(\xi). \quad (14)$$

In practice, for the sliced target distributions $\xi_{\#}Q$ whose scores must be known, it is common to instead compute the (known) score s_Q and project the result with ξ , as per the seminal work on sliced KSD [17]. Rather than performing Monte Carlo estimation, we compute the integral exactly over slices by leveraging the Cramér-Wold Theorem Thm. 6.

Theorem 9 *Let $\eta_{x' \rightarrow x} := \|x - x'\|_2^{-1}(x - x')$. Then the sliced KSD with kernel k_{gsn} is given by*

$$\begin{aligned} & \text{SKSD}^2(P, \mathcal{N}(0, \sigma^2 I_d)) \\ &= \mathbb{E}_{X, X' \sim P} \left[\left(2\gamma + \frac{X^\top X' - \eta_{X' \rightarrow X}^\top X \eta_{X' \rightarrow X}^\top X'}{\sigma^4(d-1)} \right) {}_1F_1\left(\frac{1}{2}; \frac{d}{2}; -\gamma\|X - X'\|_2^2\right) \right] \\ &+ \mathbb{E}_{X, X' \sim P} \left[\frac{1}{d} \left(\frac{\eta_{X' \rightarrow X}^\top X \eta_{X' \rightarrow X}^\top X'}{\sigma^4} - \frac{X^\top X' - \eta_{X' \rightarrow X}^\top X \eta_{X' \rightarrow X}^\top X'}{\sigma^4(d-1)} \right) {}_1F_1\left(\frac{3}{2}; \frac{d}{2} + 1; -\gamma\|X - X'\|_2^2\right) \right] \\ &+ \mathbb{E}_{X, X' \sim P} \left[\frac{1}{d} \left(\frac{2\gamma}{\sigma^2} + 4\gamma^2 \right) \|X - X'\|_2^2 {}_1F_1\left(\frac{3}{2}; \frac{d}{2} + 1; -\gamma\|X - X'\|_2^2\right) \right]. \end{aligned}$$

[Proof]

As in the case of the sliced MMD, we see that slicing once again induces heavier tails (cf. Theorem Thm. 6) in the pairwise sample comparisons though the confluent hypergeometric functions.

Finally, an unbiased U-estimator $\widehat{\text{SKSD}}$ of SKSD may be readily derived for $\widehat{P}_n = (X_i)_{i=1}^n \stackrel{\text{iid}}{\sim} P$, where $\eta_{j \rightarrow i} = \|X_i - X_j\|_2^{-1}(X_i - X_j)$,

$$\begin{aligned} & \widehat{\text{SKSD}}^2(\widehat{P}_n, \mathcal{N}(0, \sigma^2 I_d)) \\ &= \frac{1}{n(n-1)} \sum_{i=1}^n \sum_{j \neq i} \left(2\gamma + \frac{X_i^\top X_j - \eta_{j \rightarrow i}^\top X_i \eta_{j \rightarrow i}^\top X_j}{\sigma^4 (d-1)} \right) {}_1F_1\left(\frac{1}{2}; \frac{d}{2}; -\gamma \|X_i - X_j\|_2^2\right) \\ &+ \frac{1}{n(n-1)} \sum_{i=1}^n \sum_{j \neq i} \frac{1}{d} \left(\frac{\eta_{j \rightarrow i}^\top X_i \eta_{j \rightarrow i}^\top X_j}{\sigma^4} - \frac{X_i^\top X_j - \eta_{j \rightarrow i}^\top X_i \eta_{j \rightarrow i}^\top X_j}{\sigma^4 (d-1)} \right) {}_1F_1\left(\frac{3}{2}; \frac{d}{2} + 1; -\gamma \|X_i - X_j\|_2^2\right) \\ &+ \frac{1}{n(n-1)} \sum_{i=1}^n \sum_{j \neq i} \frac{1}{d} \left(\frac{2\gamma}{\sigma^2} + 4\gamma^2 \right) \|X_i - X_j\|_2^2 {}_1F_1\left(\frac{3}{2}; \frac{d}{2} + 1; -\gamma \|X_i - X_j\|_2^2\right). \end{aligned} \tag{15}$$

4 Discrepancy Regularization in Self-Supervised Learning

In this section, we study a broad family of self-supervised learning (SSL) losses spanning sliced and unsliced divergences. Regularization plays a critical role in these frameworks, as alignment objectives alone admit pathological collapse solutions. We provide a broad class of regularizers supporting various similarity measures, representation distributions, and computational considerations, and map out the corresponding tradeoffs.

We formalize the generation of views through stochastic augmentations. Let $\{x_1, \dots, x_n\}$ denote a batch of n source images. For each input, we generate a set of views by applying transformations sampled from a distribution of augmentations (comprising operations such as random cropping, color jittering, blur, grayscale, or solarization). Let $v_l^i = t_l^i(x_l)$ denote the i -th view of sample x_l , where t is a sampled augmentation. These views are processed by a neural network encoder parameterized by θ . Let $z_l^i = f_\theta(v_l^i) \in \mathbb{R}^d$ denote the final projected embedding for the i -th view of sample x_l . Here, we explicitly model the network as the composition of the backbone and projector networks where $f_\theta = f_\theta^{\text{proj}} \circ f_\theta^{\text{back}}(v)$. Let $\mathcal{P}_l := \{(v_l^i, v_l^j) : 1 \leq i < j \leq m\}$ denote the set of positive pairs for the l -th instance. If Z represents the collection of all embeddings in the batch, the batch-level self-supervised objective is:

$$\mathcal{L}(\theta) = \frac{1}{n|\mathcal{P}_l|} \sum_{l=1}^n \sum_{(i,j) \in \mathcal{P}_l} \mathcal{L}_{\text{align}}(f_\theta(v_l^i), f_\theta(v_l^j)) + \lambda \Omega(Z; Q). \tag{16}$$

Here, $\mathcal{L}_{\text{align}}$ minimizes the distance between embeddings of positive pairs, while Ω is a regularization term that prevents collapse by enforcing structure on the batch of embeddings. We formulate a general isotropic regularization loss Ω using kernel discrepancies defined by a positive definite kernel and an isotropic prior Q . In practice, we let the alignment loss be defined via the mean squared error (MSE):

$$\mathcal{L}_{\text{align}}(z_a, z_b) = \|z_a - z_b\|_2^2. \tag{17}$$

In the following sections, we specify a general family of losses under the KerJEPa framework as either *MMDReg* or *KSDReg*. We note that *analytic sliced* methods correspond to the asymptotics of infinitely sliced discrepancies presented in theorems Thm. 8 and Thm. 9 using the equivalent IMQ in place of Kummer’s function.

4.1 Sliced Discrepancy Regularization

To circumvent the computational burden of high-dimensional kernel metrics, we adopt Sliced Integral Probability Metrics (SIPMs) and mimic the structure of LeJEPa. We restrict our focus to methods that can be computed without sampling from the prior and can be approximated using numerical quadrature when defined using the metric’s spectral representation in one dimension.

This process decomposes the computational cost into two efficient steps: projections of n embeddings of dimension d onto a set of r random directions, and quadratures to estimate the spectral integral using a fixed set of u integration knots. This reduces the complexity from $\Theta(n^2 d)$ pairwise kernel evaluations to $\Theta(nr(d+u))$, making it linear in the batch size. These fast quadrature-based methods are primarily applicable when using the Gaussian or IMQ kernels combined with Gaussian, Laplace, and Student-t priors, as their spectral density, projected marginals, and CFs are analytic and well-behaved. In the case of the IMQ kernel and Student-t CF, Bessel functions only need to be computed once on their one-dimensional marginals at the known quadrature knots on initialization. We implement the two sliced methods,

termed the sliced MMDReg and sliced KSDReg, as shown in Figure Fig. 1. and we restrict our implementation to Gaussian kernel with Gaussian and Laplace priors for simplicity, as the Gaussian kernel as weighting function allows us to approximate the integral with (symmetric) Gauss-Hermite quadratures.

<pre> 1 class SlicedMMDReg(Module): 2 def __init__(self, n_knots): 3 super().__init__() 4 # Full quadrature (no symmetry assumption) 5 k, w = polynomial.hermite.hermgauss(n_knots) 6 self.knots = tensor(k * sqrt(2)).view(1,1,-1) 7 self.weights = tensor(w / sqrt(pi)).view(1,1,-1) 8 9 def target_cf(self, w, sigma, prior): 10 if prior == 'gaussian': 11 return exp(-0.5 * (sigma**2) * w**2) 12 elif prior == 'laplace': 13 return 1.0 / (1.0 + (sigma**2) * w**2) 14 15 def forward(self, z, slices, sigma, prior): 16 # Sample slices and project 17 noise = randn(slices, z.size(1)) 18 theta = normalize(noise, dim=1) 19 proj = (z @ theta.T).unsqueeze(-1) 20 21 22 # MSE ECF and CF 23 args = proj * self.knots.to(z.device) 24 emp_cf = mean(torch.cos(args), dim=0) 25 tgt_cf = self.target_cf(self.knots, sigma, prior) 26 err = (emp_cf - tgt_cf.squeeze()).pow(2) 27 28 29 # Standard integration 30 weights = self.weights.to(z.device) 31 smmd = sum(err * weights, dim=-1).mean() 32 33 return smmd </pre>	<pre> 1 class SlicedKSDReg(Module): 2 def __init__(self, n_knots): 3 super().__init__() 4 # Full quadrature (no symmetry assumption) 5 k, w = polynomial.hermite.hermgauss(n_knots) 6 self.knots = tensor(k * sqrt(2)).view(1,1,-1) 7 self.weights = tensor(w / sqrt(pi)).view(1,1,-1) 8 9 def score(self, z, sigma, prior): 10 if prior == 'gaussian': 11 return -z / sigma**2 12 elif prior == 'laplace': 13 return -normalize(z) / sigma 14 15 def forward(self, z, slices, sigma, prior): 16 # Sample slices and project 17 noise = randn(slices, z.size(1)) 18 theta = normalize(noise, dim=1) 19 proj = z @ theta.T 20 s = self.score(proj, sigma, prior) @ theta.T 21 22 # MSE Stein ECF 23 args = proj * self.knots.to(z.device) 24 w = self.knots.expand_as(args) 25 real = s * cos(args) - w * sin(args) 26 imag = s * sin(args) + w * cos(args) 27 disc = mean(real,0).pow(2) + mean(imag,0).pow(2) 28 29 # Standard integration 30 weights = self.weights.to(z.device) 31 sksd = sum(disc * weights, dim=-1).mean() 32 33 return sksd </pre>
Sliced MMDReg as generalized SIGReg	Sliced KSDReg as a Stein analogue to LeJEPa

Figure 1: Pseudo-code for the finite-sliced discrepancy regularization losses for both Gaussian and Laplace priors using the Gaussian kernel. Integration is done as Gauss-Hermite quadrature approximation.

4.2 Generalized Discrepancy Regularization

Although slicing offers computational advantages via linear-time spectral approximations, regularization can alternatively be formulated using kernels defined on the ambient high-dimensional feature space \mathbb{R}^d . Unlike sliced methods, which characterize the joint distribution via random marginal projections, these objectives minimize the discrepancy between the full empirical distribution of embeddings Z and the isotropic target prior Q using the native high-dimensional geometry, avoiding the approximation variance introduced by stochastic projections.

In the case of KSD, both Gaussian and IMQ kernels can be combined with isotropic Gaussian, Laplace, and Student-t priors. These combinations admit fully tractable closed-form expressions (provided in Appendices App. A, App. B, and §App. D), creating a flexible design space for the regularizer. This allows a practitioner to craft a Stein kernel with specific tail properties, as opposed to implicitly inducing these tails via the slicing operation. While the statistic computed in this space maintains $\Theta(n^2d)$ computational complexity, it benefits from exact computation, with approximation biases stemming only from the finite sampling of the empirical distribution of embeddings.

5 Experimental Results

We restrict our experimentation to baseline against LeJEPa on ImageNette [16] with an identical training environment. We train a ViT-s/8 on a single 80GB-A100 GPU with AdamW in BF16 across a range of MMD and KSD variants for 800 epochs on a cosine schedule with a peak learning rate of 0.0005, weight decay of 0.05 at a batch size of 256 with 4 views. We select a projector output dimension of 128 and fix the number of slices to be 1024 with 21 quadrature points to ensure best results. The augmentation pipeline is selected to mimic the example provided in LeJEPa and contains random resize crops to 128px, horizontal flips, color jitter, grayscale, blur, and solarization. We perform an ablation by performing a grid search on kernel bandwidth as well as regularization weight. We track performance with an online instance normalized linear probe and track top-1 accuracy with results reported in Table 1.

Algorithm	Type	Base Kernel	Prior	Slices	Knots	Acc. (%) \pm Std. Err.
<i>Baselines</i>						
LeJEPA	Sliced (Finite)	Gaussian	Gaussian	1024	21	91.13 \pm 0.45
MMD	Unsliced	Gaussian	Gaussian	–	–	91.29 \pm 0.45
	Sliced (Analytic)	Gaussian	Gaussian	∞	–	91.13 \pm 0.45
	Sliced (Finite)	Gaussian	Laplace	1024	21	90.25 \pm 0.47
KSD	Unsliced	Gaussian	Gaussian	–	–	91.31 \pm 0.45
	Unsliced	Gaussian	Laplace	–	–	91.18 \pm 0.45
	Unsliced	IMQ	Gaussian	–	–	91.90 \pm 0.44
	Unsliced	IMQ	Laplace	–	–	91.12 \pm 0.45
	Sliced (Analytic)	Gaussian	Gaussian	∞	–	91.11 \pm 0.45
	Sliced (Finite)	Gaussian	Gaussian	1024	21	91.36 \pm 0.45
	Sliced (Finite)	Gaussian	Laplace	1024	21	90.70 \pm 0.46

Table 1: Ablation of regularization discrepancies on ImageNette (800 epochs). We decouple the algorithm into the divergence measure, computation domain, and geometric priors. **LeJEPA** corresponds to the Epps-Pulley test, which is a finite sliced MMD with a Gaussian kernel and prior. **Type Definitions:** “Unsliced” denotes exact computation in \mathbb{R}^d ; “Sliced (Analytic)” utilizes our derived closed-form limits for infinite slices; “Sliced (Finite)” approximates the integral via Monte Carlo with 1024 random projections and 21 knots used in the quadrature.

The family of methods each perform similarly to one another, demonstrating the utility of both MMD and KSD. Given the insights from the fully analytic sliced discrepancies, we anticipate that with the proper dimension dependent bandwidth, all regularization methods are viable. In particular, we note that we did not require a heavy-tail kernel for adequate performance, despite this setting achieve the best empirical results.

We note that while the KSD naturally handles general priors, the MMD can also be adapted for non-Gaussian targets (e.g., Laplace) by approximating the spectral integral of the characteristic function via quadrature. However, this approach incurs approximation errors which depends on the number of slices and the number of integration knots used in the quadrature. Our results in Table 1 demonstrate that incorporating the Laplace prior via the quadrature estimation strategy is less accurate compared to the unsliced KSD, which targets the prior geometry directly via the score function without requiring integral approximations.

We then investigate the impact of finite slicing in relation to output dimension across training horizons using the same base setup as outlined for the MMD regularization loss (LeJEPA vs our infinite sliced equivalence). Test curves are reported in Figure Fig. 2 for complete training schedules spanning 100, 300, and 800 epochs, using 16, 128, and 1024 slices, and 16, 128, and 1024 output dimensions. We repeat the same procedure for KSD and report results in App. I

The results using both MMD (Fig. 2) and KSD (App. I) consistently demonstrate two key insights that are critical in categorizing latent embedding self-supervised algorithms. We quantify the first using the analytically sliced variation of the regularizer, which is representative of the infinitely sliced objective. Here, it is observed that the choice of projector output dimension did not impact performance. Moreover, the variance introduced via finite slicing increases with output dimension and is in accordance with our expectations (11). Insufficient slicing slows convergence and makes training less stable. In all settings, the analytically sliced variation was the top performer.

6 Discussion

The primary contribution of this work is to formalize a unified design space for these methods, providing practitioners with a toolbox of regularizers while elucidating the theoretical and computational trade-offs of each. While the introduction of KSD is novel in this context, its primary utility lies in its ability to target arbitrary priors via the score function without requiring samples, a significant advantage over MMD in certain scenarios where expectations under the prior cannot be easily computed and practitioners want to avoid approximations. In light of results, our finding inspire interesting conclusions about computational tradeoffs and the geometry of learned representations.

Computational tradeoffs. While the analytically sliced variations of MMD and KSD are robust and exhibit accelerated convergence in certain scenarios, they formally incur quadratic computational complexity and rely on large-dimension asymptotes ($d > 20$). Slicing offers linear sample complexity, but this benefit must be weighed against practical

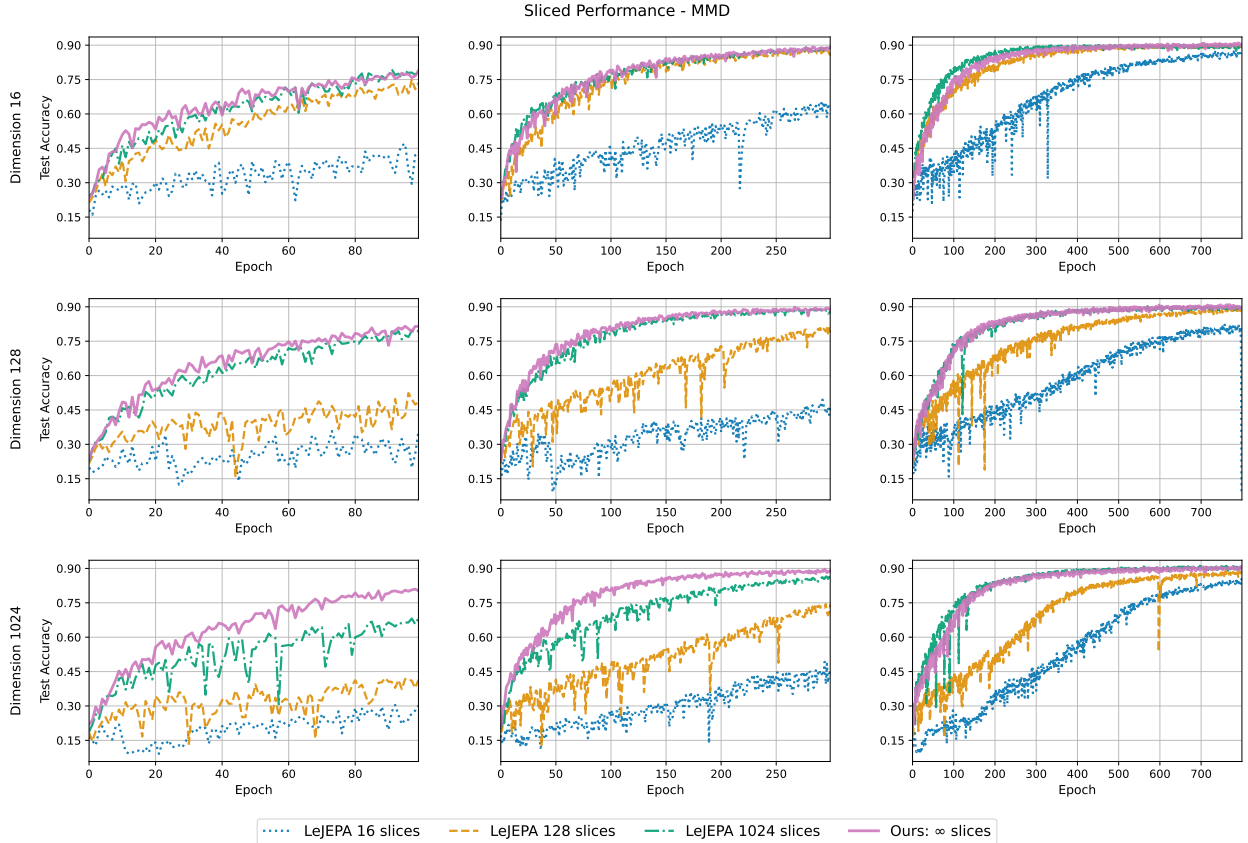


Figure 2: Impacts of slicing in various dimensions for the MMD regularizer on ImageNette, measuring test accuracy over various training horizons. Results indicate that insufficient slices slow convergence rates as a function of dimension and introduces instability in the early half of training compared to the analytically sliced counterpart.

constraints. In regimes where batch sizes do not exceed the total number of slices, the total benefit of slicing is not realized, barring any cross-device communication overhead in distributed settings. Given that these algorithms require extended training schedules, the stability of exact (or analytically sliced) methods may outweigh the theoretical speedups of finite slicing. Our theoretical results shed light on the nature of the kernels induced by slicing—particularly their heavy-tailed and dimension-dependent nature—which allows us to stabilize training and achieve faster convergence. For larger-batch settings, computation can be reduced using Random Fourier Features [23, 32, 40], MMD and KSD coresets [14, 26], or B-statistic estimators [38] that aggregate pairwise computations across distributed devices. Our experimental results show that slicing, while asymptotically more efficient in the limit of large batch size, is less stable and slower to converge on shorter training horizons.

Representation geometry. A critical consideration for these methods is their interaction with standard SSL architectures. Training employs a backbone-projector pair, where geometry is imposed on the projector’s output, yet inference relies solely on the backbone [10]. We view the projector as a non-linear pushforward map; this decoupling obscures the geometry induced at the bottleneck. Experimentally, we observe that the choice between Gaussian and Laplace priors on non-sliced experiments had negligible impact on downstream classification performance. Consequently, it remains unclear whether performance gains stem from the specific choice of isotropic prior or simply from the favorable learning dynamics of Euclidean gradients.

7 Limitations and Future Work

We acknowledge that the claims are fundamentally driven by the interpretation of results on ImageNette, which is a small dataset. Self-supervised algorithms benefit from both model and dataset scale and we aim to verify the impacts of

different variations of KerJEPa in this setting, as well as different sensitivities to kernel bandwidths. We would also like to extend the evaluation suite to include low-data finetuning, as well as transfer to detection and segmentation tasks.

References

- [1] M. Abramowitz and I. A. Stegun. *Handbook of mathematical functions with formulas, graphs, and mathematical tables*, volume 55. US Government printing office, 1948.
- [2] N. Aronszajn. Theory of reproducing kernels. *Transactions of the American Mathematical Society*, 68(3):337–404, 1950. ISSN 1088-6850. doi: 10.1090/s0002-9947-1950-0051437-7.
- [3] R. Balestrieri and Y. LeCun. LeJEPa: Provable and Scalable Self-Supervised Learning Without the Heuristics. *arXiv preprint arXiv:2511.08544*, 2025.
- [4] A. Bardes, J. Ponce, and Y. Lecun. VICReg: Variance-Invariance-Covariance Regularization For Self-Supervised Learning. In *International Conference on Learning Representations (ICLR)*, 2022.
- [5] L. Baringhaus and N. Henze. A consistent test for multivariate normality based on the empirical characteristic function. *Metrika*, 35(1):339–348, 1988. ISSN 1435-926X. doi: 10.1007/bf02613322.
- [6] A. Barp, C.-J. Simon-Gabriel, M. Girolami, and L. Mackey. Targeted separation and convergence with kernel discrepancies. *Journal of Machine Learning Research*, 25(378):1–50, 2024.
- [7] M. G. Bellemare, I. Danihelka, W. Dabney, S. Mohamed, B. Lakshminarayanan, S. Hoyer, and R. Munos. The cramer distance as a solution to biased wasserstein gradients. *arXiv preprint arXiv:1705.10743*, 2017.
- [8] C. Bonet, P. Berg, N. Courty, F. Septier, L. Drumetz, and M.-T. Pham. Spherical sliced-wasserstein. In *International Conference on Learning Representations (ICLR)*, 2023.
- [9] N. Bonneel, J. Rabin, G. Peyré, and H. Pfister. Sliced and Radon Wasserstein barycenters of measures. *Journal of Mathematical Imaging and Vision*, 51(1):22–45, 2015.
- [10] F. Bordes, R. Balestrieri, Q. Garrido, A. Bardes, and P. Vincent. Guillotine regularization: Why removing layers is needed to improve generalization in self-supervised learning. *Transactions on Machine Learning Research*, 2023. ISSN 2835-8856.
- [11] M. Caron, I. Misra, J. Mairal, P. Goyal, P. Bojanowski, and A. Joulin. Unsupervised learning of visual features by contrasting cluster assignments. In *Advances in Neural Information Processing Systems (NeurIPS)*, volume 33, pages 9912–9924, 2020.
- [12] T. Chen, S. Kornblith, M. Norouzi, and G. Hinton. A simple framework for contrastive learning of visual representations. In *International Conference on Machine Learning (ICML)*, volume 119, pages 1597–1607. PMLR, 2020.
- [13] K. Chwialkowski, H. Strathmann, and A. Gretton. A kernel test of goodness of fit. In *International Conference on Machine Learning (ICML)*, volume 48, pages 2606–2615. PMLR, 2016.
- [14] C. Domingo-Enrich, R. Dwivedi, and L. Mackey. Compress then test: Powerful kernel testing in near-linear time. In F. Ruiz, J. Dy, and J.-W. van de Meent, editors, *International Conference on Artificial Intelligence and Statistics (AISTATS)*, volume 206, pages 1174–1218. PMLR, 2023.
- [15] T. W. Epps and L. B. Pulley. A test for normality based on the empirical characteristic function. *Biometrika*, 70(3):723–726, 1983. ISSN 00063444.
- [16] fast.ai. imagenette, 2019. URL <https://github.com/fastai/imagenette>.
- [17] W. Gong, Y. Li, and J. M. Hernández-Lobato. Sliced kernelized Stein discrepancy. In *International Conference on Learning Representations (ICLR)*, 2021.
- [18] J. Gorham and L. Mackey. Measuring sample quality with Stein's method. In *Advances in Neural Information Processing Systems (NeurIPS)*, volume 28, 2015.
- [19] J. Gorham and L. Mackey. Measuring sample quality with kernels. In *International Conference on Machine Learning (ICML)*, volume 70, pages 1292–1301. PMLR, 2017.
- [20] A. Gretton, K. M. Borgwardt, M. J. Rasch, B. Schölkopf, and A. Smola. A kernel two-sample test. *Journal of Machine Learning Research*, 13(25):723–773, 2012.
- [21] J.-B. Grill, F. Strub, F. Althé, C. Tallec, P. Richemond, E. Buchatskaya, C. Doersch, B. Avila Pires, Z. Guo, M. Gheshlaghi Azar, B. Piot, k. kavukcuoglu, R. Munos, and M. Valko. Bootstrap your own latent - a new approach to self-supervised learning. In H. Larochelle, M. Ranzato, R. Hadsell, M. Balcan, and H. Lin, editors, *Advances in Neural Information Processing Systems (NeurIPS)*, volume 33, pages 21271–21284, 2020.

- [22] K. He, H. Fan, Y. Wu, S. Xie, and R. Girshick. Momentum contrast for unsupervised visual representation learning. In *Proceedings of the IEEE/CVF Conference on Computer Vision and Pattern Recognition (CVPR)*, 2020.
- [23] J. Huggins and L. Mackey. Random feature Stein discrepancies. In *Advances in Neural Information Processing Systems (NeurIPS)*, volume 31, 2018.
- [24] S. Knop, P. Spurek, J. Tabor, I. Podolak, M. Mazur, and S. Jastrzebski. Cramer-Wold auto-encoder. *Journal of Machine Learning Research*, 21(164):1–28, 2020.
- [25] A. Korba, P.-C. Aubin-Frankowski, S. Majewski, and P. Ablin. Kernel Stein discrepancy descent. In *International Conference on Machine Learning (ICML)*, volume 139, pages 5719–5730. PMLR, 2021.
- [26] L. Li, R. Dwivedi, and L. Mackey. Debiased distribution compression. In *International Conference on Machine Learning (ICML)*, volume 235, pages 27675–27731. PMLR, 2024.
- [27] Y. Li, R. Pogodin, D. J. Sutherland, and A. Gretton. Self-supervised learning with kernel dependence maximization. In *Advances in Neural Information Processing Systems (NeurIPS)*, volume 34, pages 15543–15556, 2021.
- [28] Q. Liu, J. Lee, and M. Jordan. A kernelized Stein discrepancy for goodness-of-fit tests. In *International Conference on Machine Learning (ICML)*, volume 48, pages 276–284. PMLR, 2016.
- [29] T. Moutakanni, M. Oquab, M. Szafraniec, M. Vakalopoulou, and P. Bojanowski. You don’t need domain-specific data augmentations when scaling self-supervised learning. In *Advances in Neural Information Processing Systems (NeurIPS)*, volume 37, pages 116106–116125, 2024.
- [30] K. Nadjahi, A. Durmus, L. Chizat, S. Kolouri, S. Shahrapour, and U. Simsekli. Statistical and topological properties of sliced probability divergences. In *Advances in Neural Information Processing Systems (NeurIPS)*, volume 33, pages 20802–20812, 2020.
- [31] J. Rabin, G. Peyré, J. Delon, and M. Berton. Wasserstein barycenter and its application to texture mixing. In A. M. Bruckstein, B. M. ter Haar Romeny, A. M. Bronstein, and M. M. Bronstein, editors, *Scale Space and Variational Methods in Computer Vision*, pages 435–446, Berlin, Heidelberg, 2012. Springer Berlin Heidelberg. ISBN 978-3-642-24785-9.
- [32] A. Rahimi and B. Recht. Random features for large-scale kernel machines. In *Advances in Neural Information Processing Systems (NeurIPS)*, volume 20, 2007.
- [33] C. E. Rasmussen and C. K. I. Williams. *Gaussian Processes for Machine Learning*. The MIT Press, 2005. ISBN 9780262256834. doi: 10.7551/mitpress/3206.001.0001.
- [34] H. Sepanj and P. Fieguth. Aligning feature distributions in vicreg using maximum mean discrepancy for enhanced manifold awareness in self-supervised representation learning. *Journal of Computational Vision and Imaging Systems*, 10(1):13–18, Feb. 2025. doi: 10.15353/jcvis.v10i1.10002.
- [35] B. K. Sriperumbudur, A. Gretton, K. Fukumizu, B. Schölkopf, and G. R. Lanckriet. Hilbert space embeddings and metrics on probability measures. *Journal of Machine Learning Research*, 11(50):1517–1561, 2010.
- [36] C. Villani et al. *Optimal transport: old and new*, volume 338. Springer, 2008.
- [37] T. Wang and P. Isola. Understanding contrastive representation learning through alignment and uniformity on the hypersphere. In *International Conference on Machine Learning (ICML)*, volume 119, pages 9929–9939. PMLR, 2020.
- [38] W. Zaremba, A. Gretton, and M. Blaschko. B-test: A non-parametric, low variance kernel two-sample test. In *Advances in Neural Information Processing Systems (NeurIPS)*, volume 26, 2013.
- [39] J. Zbontar, L. Jing, I. Misra, Y. LeCun, and S. Deny. Barlow twins: Self-supervised learning via redundancy reduction. In *International Conference on Machine Learning (ICML)*, volume 139, pages 12310–12320. PMLR, 2021.
- [40] J. Zhao and D. Meng. FastMMD: Ensemble of circular discrepancy for efficient two-sample test. *Neural Computation*, 27(6):1345–1372, 2015. doi: 10.1162/NECO_a_00732.

A Shift-Invariant Kernels

A common shift-invariant kernel of interest, categorized by its fast decay profile is the Gaussian Kernel

$$k_{\text{gsn}}(x, y) = \exp(-\gamma\|x - y\|_2^2), \quad \rho_{\text{gsn}}(\omega) = \frac{1}{(4\pi\gamma)^{d/2}} \exp\left(-\frac{1}{4\gamma}\|\omega\|_2^2\right). \quad (18)$$

Here, the bandwidth $\gamma > 0$ controls smoothness between global and local dependencies between samples.

We draw attention to a family of kernels of interest, namely, the *Inverse Multiquadric Kernel* (IMQ). Unlike the Gaussian kernel, which has exponentially decaying tails, the IMQ decays at a polynomial rate (heavy-tailed) and is defined as

$$k_{\text{imq}}(x, y) = (1 + \alpha\|x - y\|_2^2)^{-\beta}, \quad \rho_{\text{imq}}(\omega) = \frac{2^{1-\beta}}{\Gamma(\beta)(2\pi\alpha)^{d/2}} \left(\frac{\|\omega\|_2}{2\sqrt{\alpha}}\right)^\nu K_\nu\left(\frac{\|\omega\|_2}{\sqrt{\alpha}}\right), \quad (19)$$

where Γ is the Gamma function and K_ν is the modified Bessel of second kind, order ν . The parameter $\beta > 0$ acts as a shape parameter that determines the heaviness of the tails (the rate of polynomial decay), while $\alpha > 0$ serves as the inverse length scale. The IMQ kernel can be interpreted as an infinite scale mixture of Gaussian kernels. This heavy-tailed property allows it to capture long-range dependencies and maintain gradient signals in the tails, which are often missed by the fixed-scale Gaussian kernel.

B Isotropic Prior Distributions

There are three isotropic priors of interest to be used as a regularizer that include the Gaussian, Laplace, and Student-t distributions. Their definitions and score functions are defined in the table as follows:

Distribution	Notation	$p(x)$	$\nabla_x \log p(x)$	$\phi(\omega)$
Gaussian	$\mathcal{N}(0, \sigma^2 I_d)$	$\frac{1}{(2\pi\sigma^2)^{d/2}} \exp\left(-\frac{1}{2\sigma^2}\ x\ _2^2\right)$	$-\frac{1}{\sigma^2}x$	$\exp\left(-\frac{1}{2}\sigma^2\ \omega\ _2^2\right)$
Laplace	$\text{Lap}(0, \sigma I_d)$	$\frac{\Gamma(d/2)}{2\pi^{d/2}\sigma^d\Gamma(d)} \exp\left(-\frac{1}{\sigma}\ x\ _2\right)$	$-\frac{1}{\sigma} \frac{x}{\ x\ _2}$	$(1 + \sigma^2\ \omega\ _2^2)^{-\frac{d+1}{2}}$
Student-t	$\mathcal{T}_\nu(0, \sigma^2 I_d)$	$\frac{\Gamma(\frac{\nu+d}{2})}{\Gamma(\frac{\nu}{2})(\nu\pi\sigma^2)^{d/2}} \left(1 + \frac{1}{\nu\sigma^2}\ x\ _2^2\right)^{-\frac{\nu+d}{2}}$	$-\frac{\nu+d}{\nu\sigma^2 + \ x\ _2^2}x$	$\frac{K_{\nu/2}(\sqrt{\nu}\sigma\ \omega\ _2)(\sqrt{\nu}\sigma\ \omega\ _2)^{\nu/2}}{\Gamma(\nu/2)2^{\nu/2-1}}$

Table 2: Isotropic prior distributions: definitions, scores, and characteristic functions.

C Maximum Mean Discrepancy

In this section, we derive variations of the MMD and corresponding sample-based estimators, discussing the features and difficulties associated with different choices of kernels and priors. Altogether, we provide the following MMD estimators, with n, m denoting the number of samples drawn from the distribution under test and the prior distribution respectively:

1. $\widehat{\text{UMMD}}_{k,n,m}^2$ (cf. (21)): a general unbiased estimator for MMDs with arbitrary kernels and priors;
2. $\widehat{\text{CMMD}}_{k,n}^2$ (cf. (22)): a consistent estimator for shift-invariant kernels k and priors with known characteristic functions, which requires only $O(n)$ computational complexity; and
3. $\widehat{\text{UGMMD}}_{\sigma^2,n}^2$ (cf. (24)): an unbiased estimator for Gaussian kernels with prior $\mathcal{N}(0, \sigma^2 I_d)$, with reduced variance.

To begin, we recall the definition of the MMD with positive definite kernel k ,

$$\text{MMD}_k^2(P, Q) = \mathbb{E}_{X, X' \sim P}[k(X, X')] + \mathbb{E}_{Y, Y' \sim Q}[k(Y, Y')] - 2\mathbb{E}_{(X, Y) \sim P \otimes Q}[k(X, Y)]. \quad (20)$$

The following U-statistic is an unbiased estimator [20] of the MMD,

$$\widehat{\text{UMMD}}_{k,n,m}^2(P, Q) = \frac{1}{n(n-1)} \sum_{i=1}^n \sum_{j \neq i}^n k(X_i, X_j) + \frac{1}{m(m-1)} \sum_{i=1}^m \sum_{j \neq i}^m k(Y_i, Y_j) - 2 \sum_{i=1}^n \sum_{j=1}^m k(X_i, Y_j), \quad (21)$$

$$X_i \stackrel{\text{iid}}{\sim} P \quad \text{and} \quad Y_i \stackrel{\text{iid}}{\sim} Q.$$

It is well-known that estimation of the MMD via this U-statistic achieves dimension-free sample complexity [20]. However, there are at least two qualities of this estimator one might hope to improve:

1. It involves pairwise kernel evaluations, which scales quadratically with the number of samples drawn from the distributions under comparison; and
2. If one could compute the expectations over the prior (Q) in closed form, variance can be reduced.

With regard to the first point, we can turn to the Bochner integral formulation of the MMD, which would scale linearly with the number of samples. Particularly, we derive the CF MMD estimator (a V-estimator) below:

$$\widehat{\text{CMMD}}_{k,n}^2(P, Q) = \int_{\mathbb{R}^d} |\phi_{\hat{P}_n}(\omega) - \phi_Q(\omega)|^2 \rho_k(\omega) d\omega, \quad \hat{P}_n = \frac{1}{n} \sum_{i=1}^n \delta_{X_i}, \quad X_i \stackrel{\text{iid}}{\sim} P, \quad (22)$$

where ϕ_P denotes the CF of the probability measure P . Notably, under this estimator, there are no pairwise comparisons being made, and the complexity scales only as $O(n)$. Here, we assume that ϕ_Q is known analytically, which is often the case for priors used in practice (e.g. Gaussian, Laplace, or Student-t priors). Note, however, that certain kernels (e.g. Student-t, IMQ) require their own quadrature for estimating their spectral density, adding additional overhead, which also scales with d .

With regard to the second criterion, computing the expectation over Q in closed form is generally intractable. Exceptionally, this can be done in the scenario of Gaussian priors under Gaussian kernels.

Proposition 10 *For any distribution $P \in \mathcal{P}(\mathbb{R}^d)$, we have*

$$\text{MMD}_{k_{\text{gsn}}}^2(P, \mathcal{N}(0, \sigma^2 I_d)) = \mathbb{E}_{X, X' \sim P} \exp(-\gamma \|X - X'\|_2^2) - \frac{2}{(1 + 2\gamma\sigma^2)^{d/2}} \mathbb{E}_{X \sim P} \exp\left(-\frac{\gamma}{1 + 2\gamma\sigma^2} \|X\|_2^2\right) + C_{\gamma, \sigma, d}^{\text{gauss}}, \quad (23)$$

for a constant $C_{\gamma, \sigma, d}^{\text{gauss}}$ independent of P given by

$$C_{\gamma, \sigma, d}^{\text{gauss}} := \frac{1}{(1 + 4\gamma\sigma^2)^{d/2}}.$$

We prove this proposition below. First, we highlight the resulting unbiased U-statistic $\widehat{\text{UGMMD}}_{\sigma^2, n}^2(P)$ in the case of a Gaussian prior with a Gaussian kernel—this is also known as the *BHEP* estimator [5]:

$$\widehat{\text{UGMMD}}_{\sigma^2, n}^2(P) = \frac{1}{n(n-1)} \sum_{i=1}^n \sum_{j \neq i}^n \exp(-\gamma \|X_i - X_j\|_2^2) - \frac{2}{(1 + 2\gamma\sigma^2)^{d/2}} \sum_{i=1}^n \exp\left(-\frac{\gamma}{1 + 2\gamma\sigma^2} \|X_i\|_2^2\right) + C_{\gamma, \sigma, d}^{\text{gauss}}, \quad (24)$$

where $\{X_i\}_{i=1}^n \stackrel{\text{iid}}{\sim} P$, and where $C_{\gamma, \sigma, d}^{\text{gauss}}$ is independent of P and given in Proposition Thm. 10.

Proof *Proof of Proposition Thm. 10.* Let $N = \mathcal{N}(0, \sigma^2 I_d)$. Starting from (20), we have

$$\text{MMD}_{k_{\text{gsn}}}^2(P, N) = \mathbb{E}_{X, X' \sim P} \exp(-\gamma \|X - X'\|_2^2) + \underbrace{\mathbb{E}_{Y, Y' \sim N} [k_{\text{gsn}}(Y, Y')]}_A - 2 \underbrace{\mathbb{E}_{(X, Y) \sim P \otimes N} [k(X, Y)]}_B.$$

We simplify terms A and B individually. Starting with A,

$$\begin{aligned} A &:= \mathbb{E}_{Y, Y' \sim Q} [k_{\text{gsn}}(Y, Y')] \\ &= \int_{\mathbb{R}^d} \int_{\mathbb{R}^d} \exp(-\gamma \|y - y'\|_2^2) \frac{1}{(2\pi\sigma^2)^d} \exp\left(-\frac{1}{2\sigma^2} (\|y\|_2^2 + \|y'\|_2^2)\right) dy dy' \\ &= \frac{1}{(1 + 4\gamma\sigma^2)^{d/2}} =: C_{\gamma, \sigma, d}^{\text{gauss}}. \end{aligned}$$

Now, for B, we have

$$\mathbb{E}_{Y \sim N}[k_{\text{gsn}}(x, Y)] = \int_{\mathbb{R}^d} \exp(-\gamma \|x - y\|_2^2) \frac{1}{(2\pi\sigma^2)^{d/2}} \exp\left(-\frac{1}{2\sigma^2} \|y\|_2^2\right) dy.$$

This is a convolution of Gaussians, which evaluates to

$$\mathbb{E}_{Y \sim N}[k_{\text{gsn}}(x, Y)] = \frac{1}{(2\gamma\sigma^2 + 1)^{d/2}} \exp\left(-\frac{\gamma}{2\gamma\sigma^2 + 1} \|x\|_2^2\right).$$

Substituting into B, we have

$$\begin{aligned} B &:= \mathbb{E}_{X \sim P} \mathbb{E}_{Y \sim N}[k_{\text{gsn}}(X, Y)] \\ &= \frac{1}{(2\gamma\sigma^2 + 1)^{d/2}} \mathbb{E}_{X \sim P} \left[\exp\left(-\frac{\gamma}{2\gamma\sigma^2 + 1} \|X\|_2^2\right) \right]. \end{aligned}$$

Substituting A and B above completes the proof. ■

D Kernel Stein Discrepancy

We derive variations of the KSD under different kernels and priors incorporated via score function. We let $\{X_1, \dots, X_n\} \in \mathbb{R}^d$ be independent samples from an arbitrary empirical distribution P resulting in an empirical distribution $\hat{P} = n^{-1} \sum_{i=1}^n \delta_{X_i}$, Q be a target isotropic prior distribution with score function s_Q , and consider a positive-definite kernel $k : \mathbb{R}^d \times \mathbb{R}^d \rightarrow \mathbb{R}$ with associated RKHS \mathcal{H} . An unbiased U-statistic for the squared KSD is given by

$$\widehat{\text{KSD}}^2(P, Q) = \frac{1}{n(n-1)} \sum_{i=1}^n \sum_{j \neq i} k_{\text{stein}}(X_i, X_j), \quad (25)$$

where the Stein kernel is defined as

$$k_{\text{stein}}(x, y) = s_Q(x)^\top k(x, y) s_Q(y) + s_Q(x)^\top \nabla_y k(x, y) + \nabla_x k(x, y)^\top s_Q(y) + \text{tr}(\nabla_x \nabla_y^\top k(x, y)). \quad (26)$$

We provide a table with gradients and Hessians for the Gaussian and IMQ kernels needed to assemble the discrepancy, noting that the gradients for a radial kernel are odd ($\nabla_x k(x, y) = -\nabla_y k(x, y)$).

$k(x, y)$	$\nabla_x k(x, y)$	$\text{tr}(\nabla_x \nabla_y k(x, y))$
Gaussian	$-2\gamma(x - y) \exp(-\gamma \ x - y\ _2^2)$	$(2\gamma d - 4\gamma^2 \ x - y\ _2^2) \exp(-\gamma \ x - y\ _2^2)$
IMQ	$-2\alpha\beta(x - y)(1 + \alpha \ x - y\ _2^2)^{-(\beta+1)}$	$4\alpha^2\beta(\beta + 1) \ x - y\ _2^2 (1 + \alpha \ x - y\ _2^2)^{-(\beta+2)}$
Bochner	$\int_{\mathbb{R}^d} i\omega \exp(i\omega^\top(x - y)) \rho(\omega) d\omega$	$\int_{\mathbb{R}^d} \ \omega\ _2^2 \exp(i\omega^\top(x - y)) \rho(\omega) d\omega$

Table 3: Gradients and Hessians for the Gaussian, IMQ, and general shift-invariant kernels used to derive closed-form Stein kernels

It is clear that all combinations of kernel gradients and Hessians can be combined with priors App. B to formulate closed-form Stein kernels which do not require sampling from the prior. We now provide the spectral and non-spectral forms of the squared KSD, given that finding closed-form expression of the estimator is trivial due to the incorporation of the prior via score function.

D.1 Spectral Representations of KSD

We derive the general spectral decomposition of the squared KSD for generic score function s_Q .

Proposition 11 For a probability distribution Q , let s_Q denote its score $\nabla \log Q$. For any shift-invariant kernel k ,

$$\text{KSD}_k^2(P, Q) = \int_{\mathbb{R}^d} \left\| \mathbb{E}_{X \sim P} [(s_Q(X) + i\omega) \exp(i\omega^\top X)] \right\|^2 \rho_k(\omega) d\omega,$$

where ρ_k is the spectral density of the kernel k . [Source]

Proof Recalling the definition of the Stein Kernel and using the general Fourier representation of a shift-invariant kernel under Bochner's theorem, we substitute the gradients and Hessian provided in section App. D and group terms under the integral such that

$$\begin{aligned} k_{\text{stein}}(x, x') &= \int_{\mathbb{R}^d} [s_Q(x)^\top s_Q(x') - i s_Q(x)^\top \omega + i \omega^\top s_Q(x') + \omega^\top \omega] \exp(i\omega^\top x) \exp(-i\omega^\top x') \rho(\omega) d\omega \\ &= \int_{\mathbb{R}^d} (s_Q(x) + i\omega)^\top (s_Q(x') - i\omega) \exp(i\omega^\top (x - x')) \rho_k(\omega) d\omega. \end{aligned} \quad (27)$$

Taking the expectation $\mathbb{E}_{x, x' \sim P}$ and noting that $s_Q(x) - i\omega$ is the complex conjugate of $s_Q(x) + i\omega$, we may write the squared KSD as

$$\text{KSD}_k^2(P, Q) = \int_{\mathbb{R}^d} \left\| \mathbb{E}_{X \sim P} [(s_Q(X) + i\omega) \exp(i\omega^\top X)] \right\|^2 \rho_k(\omega) d\omega. \quad (28)$$

■

Corollary 12 For any shift-invariant kernel k , it holds that

$$\text{KSD}_k^2(P, \mathcal{N}(0, \sigma^2 I_d)) = \int_{\mathbb{R}^d} \left\| \omega \phi_P(\omega) + \frac{1}{\sigma^2} \nabla_\omega \phi_P(\omega) \right\|^2 \rho_k(\omega) d\omega,$$

where ϕ_P is the CF of the distribution P . [Source]

Proof Let $N := \mathcal{N}(0, \sigma^2 I_d)$, and note that $s_N(x) = -x/\sigma^2$. Substituting into Proposition Thm. 4,

$$\begin{aligned} \text{KSD}_k^2(P, N) &= \int_{\mathbb{R}^d} \left\| \mathbb{E}_{X \sim P} \left[\left(i\omega - \frac{X}{\sigma^2} \right) \exp(i\omega^\top X) \right] \right\|^2 \rho_k(\omega) d\omega \\ &= \int_{\mathbb{R}^d} \left\| i\omega \phi_P(\omega) - \frac{1}{\sigma^2} \mathbb{E}_{X \sim P} [X \exp(i\omega^\top X)] \right\|^2 \rho_k(\omega) d\omega. \end{aligned}$$

Using the identity that $\mathbb{E}[X e^{i\omega^\top X}] = -i \nabla \phi_P(\omega)$, we have

$$\begin{aligned} \text{KSD}_k^2(P, N) &= \int_{\mathbb{R}^d} \left\| i\omega \phi_P(\omega) + \frac{i}{\sigma^2} \nabla \phi_P(\omega) \right\|^2 \rho_k(\omega) d\omega \\ &= \int_{\mathbb{R}^d} \left\| \omega \phi_P(\omega) + \frac{1}{\sigma^2} \nabla \phi_P(\omega) \right\|^2 \rho_k(\omega) d\omega. \end{aligned}$$

■

E Sliced Maximum Mean Discrepancies without Slicing with an Isotropic Gaussian Prior

Theorem 7 Let $\text{SIGReg} : \mathcal{P}(\mathbb{R}^d) \rightarrow \mathbb{R}_+$ denote the SIGReg regularizer [3]; that is,

$$\text{SIGReg}(P) := \mathbb{E}_{\xi \sim \mathcal{U}(\mathbb{S}^{d-1})} [n^{-1} \text{EP}(\xi^\top P)].$$

It holds that SIGReg is equivalent to a particular MMD,

$$\text{SIGReg}(P) = \text{MMD}_{\kappa_d}^2(P, \mathcal{N}(0, \sigma^2 I_d)), \quad \kappa_d(x, y) := {}_1F_1\left(\frac{1}{2}; \frac{d}{2}; -\gamma \|x - y\|_2^2\right),$$

where ${}_1F_1$ is the Kummer Confluent Hypergeometric function, and MMD_k denotes the MMD under the kernel k . Particularly, κ_d has polynomially decaying tails (as opposed to exponentially decaying tails like k_{gsn}). [Source]

Proof As we saw in §Sec. 3.2.1, it holds that

$$\mathbb{E}P(P) = n\text{MMD}_{k_{\text{gsn}}}^2(P, \mathcal{N}(0, \sigma^2)).$$

Let $X \sim P$ and $N \sim \mathcal{N}(0, \sigma^2 I_d)$. Then, by the linearity of the expectation, we have

$$\begin{aligned} \text{SIGReg}(P) &= \mathbb{E}_{\xi \sim \mathcal{U}(\mathbb{S}^{d-1})} \left[\text{MMD}_{k_{\text{gsn}}}^2(\xi^\top P, \xi^\top \mathcal{N}(0, \sigma^2 I_d)) \right] \\ &= \mathbb{E}_{X, X' \sim P} \mathbb{E}_{\xi \sim \mathcal{U}(\mathbb{S}^{d-1})} k_{\text{gsn}}(\xi^\top X, \xi^\top X') + \mathbb{E}_{Y, Y' \sim \mathcal{N}(0, \sigma^2 I_d)} \mathbb{E}_{\xi \sim \mathcal{U}(\mathbb{S}^{d-1})} k_{\text{gsn}}(\xi^\top Y, \xi^\top Y') \\ &\quad - 2\mathbb{E}_{X \sim P, Y \sim \mathcal{N}(0, \sigma^2 I_d)} \mathbb{E}_{\xi \sim \mathcal{U}(\mathbb{S}^{d-1})} k_{\text{gsn}}(\xi^\top X, \xi^\top Y). \end{aligned}$$

Moreover, by [30, Corollary S3], it holds that $(x, y) \mapsto \mathbb{E}_{\xi \sim \mathcal{U}(\mathbb{S}^{d-1})} k_{\text{gsn}}(\xi^\top x, \xi^\top y) = {}_1F_1(1/2; d/2; \gamma \|x - y\|_2^2)$ is a particular solution to *Kummer's equation*; that is, ${}_1F_1(a, b, z)$ is a solution to

$$z \frac{d^2 w}{dz^2} + (b - z) \frac{dw}{dz} - \alpha w = 0.$$

Thus, substituting, we have

$$\begin{aligned} \text{SIGReg}(P) &= \mathbb{E}_{X, X' \sim P} \left[{}_1F_1\left(\frac{1}{2}; \frac{d}{2}; \gamma \|X - X'\|_2^2\right) \right] + \mathbb{E}_{Y, Y' \sim \mathcal{N}(0, \sigma^2 I_d)} \left[{}_1F_1\left(\frac{1}{2}; \frac{d}{2}; \gamma \|Y - Y'\|_2^2\right) \right] \\ &\quad - 2\mathbb{E}_{X \sim P, Y \sim \mathcal{N}(0, \sigma^2 I_d)} \left[{}_1F_1\left(\frac{1}{2}; \frac{d}{2}; \gamma \|X - Y\|_2^2\right) \right] \\ &\equiv \text{MMD}_{\kappa_d}^2(P, \mathcal{N}(0, \sigma^2 I_d)). \end{aligned}$$

This proves the first claim. Next, it is known [1, Chapter 13] that for fixed d ,

$${}_1F_1\left(\frac{1}{2}; \frac{d}{2}; -\gamma \|x - y\|_2^2\right) \sim \Gamma\left(\frac{d}{2}\right) \left[\frac{1}{\Gamma(1/2)} \exp(-\gamma \|x - y\|_2^2) (-\gamma \|x - y\|_2^2)^{(1-d)/2} + \frac{1}{\Gamma((d-1)/2)} \gamma^{-1/2} \|x - y\|_2^{-1} \right],$$

where $f(\xi) \sim g(\xi)$ denotes that f is asymptotically equivalent to g in ξ , in the sense that $\lim_{\xi \rightarrow \infty} f(\xi)/g(\xi) = 1$; the expression above is stated asymptotically for $\|x - y\|_2$. Thus, directly we have that the final term dominates for large $\|x - y\|_2$, and it follows that for $d > 1$, $\kappa_d(x, y)$ decays like $\Gamma((d-1)/2)^{-1} \gamma^{-1/2} \|x - y\|_2^{-1}$. ■

Theorem 8 Let $P \in \mathcal{P}(\mathbb{R}^d)$, and let $\hat{P}_n := (X_i)_{i=1}^n \stackrel{\text{iid}}{\sim} P$. Define the estimator $\widehat{\text{MMD-Gauss}}_{\kappa_d} : \mathbb{R}^{d \times n} \rightarrow \mathbb{R}_+$ according to

$$\widehat{\text{MMD-Gauss}}_{\kappa_d}^2(\hat{P}_n) := \frac{1}{n(n-1)} \sum_{i=1}^n \sum_{j \neq i} \kappa_d(X_i, X_j) - \frac{2}{n\sqrt{1+2\gamma\sigma^2}} \sum_{i=1}^n {}_1F_1\left(\frac{1}{2}; \frac{d}{2}; -\frac{\gamma}{1+2\gamma\sigma^2} \|X_i\|_2^2\right) + C \quad (12)$$

for some constant C independent of P . Then $\widehat{\text{MMD-Gauss}}_{\kappa_d}^2(\hat{P}_n)$ is an unbiased estimate of $\text{SIGReg}(P)$, and $|\mathbb{E}[\widehat{\text{MMD-Gauss}}_{\kappa_d}^2(\hat{P}_n) - \text{SIGReg}(\hat{P}_n)]| \leq O(1/n)$. [\[Source\]](#)

Proof The proof is a direct computation. By Theorem Thm. 7, $\text{SIGReg}(P) = \text{MMD}_{\kappa_d}^2(P, \mathcal{N}(0, \sigma^2))$, and we will show that $\widehat{\text{MMD-Gauss}}_{\kappa_d}^2(\hat{P}_n)$ is the (unbiased) U-statistic $\widehat{\text{U-MMD}}_{\kappa_d}^2$ for $\text{MMD}_{\kappa_d}^2(P, \mathcal{N}(0, \sigma^2))$. This U-statistic will be derived by integrating the contributions of $\mathcal{N}(0, 1)$ in closed form instead of sampling. By [20], denoting $N = \mathcal{N}(0, \sigma^2)$, we have

$$\widehat{\text{U-MMD}}_{\kappa_d}^2(\hat{P}_n, N) = \underbrace{\frac{1}{n(n-1)} \sum_{i=1}^n \sum_{j \neq i} \kappa_d(X_i, X_j)}_{\text{I}} + \underbrace{\iint \kappa_d(y_1, y_2) dN(y_1) dN(y_2)}_{\text{II}:=C} - \underbrace{\frac{2}{n} \sum_{i=1}^n \int \kappa_d(X_i, y) dN(y)}_{\text{III}}.$$

Note that term II is totally independent of P , so we write it off as a constant C . The term I above is expressed solely in terms of pairwise kernel evaluations from samples from P , it will not be simplified further. To complete the proof, it

remains to simplify III. Unpacking κ_d into an expectation over uniform random projections, we have

$$\begin{aligned} \text{III} &= \frac{2}{n} \sum_{i=1}^n \int_{\mathbb{S}^{d-1}} \int_{\mathbb{R}} \exp(-\gamma(\xi^\top(X_i - y))^2) \frac{1}{\sqrt{2\pi}\sigma} \exp(-\frac{1}{2\sigma^2}(\xi^\top y)^2) dy d\mathcal{U}(\xi) \\ &\stackrel{(*)}{=} \frac{2}{n} \frac{1}{\sqrt{2\gamma\sigma^2}} \sum_{i=1}^n \int_{\mathbb{S}^{d-1}} \exp\left(-\frac{\gamma(\xi^\top X_i)^2}{1+2\gamma\sigma^2}\right) d\mathcal{U}(\xi) \\ &= \frac{2}{n\sqrt{1+2\gamma\sigma^2}} \sum_{i=1}^n {}_1F_1\left(\frac{1}{2}; \frac{d}{2}; -\frac{\gamma}{1+2\gamma\sigma^2}\|X_i\|_2\right). \end{aligned}$$

In the previous computation, step (*) simply computes the expectation of $\exp(-\gamma Z^2)$, for $Z := \xi^\top(X_i - y)$, which is a Gaussian scalar random variable. Summing I, this expression for III, and C , we find that indeed $\widehat{\text{MMD-Gauss}}_{\kappa_d}^2(\widehat{P}_n)$ is an unbiased estimator of $\text{SIGReg}(P)$ as a U-statistic of $\text{MMD}_{\kappa_d}^2(P, \mathcal{N}(0, \sigma^2))$.

For the final claim, it was shown in [3, Theorem 6] that

$$\left| \mathbb{E} \left[\widehat{\text{SIGReg}}(\widehat{P}_n) - \text{SIGReg}(P) \right] \right| \leq O(1/n).$$

Therefore, we immediately have

$$\begin{aligned} \left| \mathbb{E} \left[\widehat{\text{MMD-Gauss}}_{\kappa_d}^2(\widehat{P}_n) - \widehat{\text{SIGReg}}(\widehat{P}_n) \right] \right| &= \left| \mathbb{E} \left[\widehat{\text{MMD-Gauss}}_{\kappa_d}^2(\widehat{P}_n) - \text{SIGReg}(P) \right] + \mathbb{E} \left[\text{SIGReg}(P) - \widehat{\text{SIGReg}}(\widehat{P}_n) \right] \right| \\ &= \left| \mathbb{E} \left[\text{SIGReg}(P) - \widehat{\text{SIGReg}}(\widehat{P}_n) \right] \right| \leq O(1/n), \end{aligned}$$

which completes the proof. ■

F Sliced Kernel Stein Discrepancies without Slicing with an Isotropic Gaussian Prior

Theorem 9 Let $\eta_{x' \rightarrow x} := \|x - x'\|_2^{-1}(x - x')$. Then the sliced KSD with kernel k_{gsn} is given by

$$\begin{aligned} \text{SKSD}^2(P, \mathcal{N}(0, \sigma^2 I_d)) &= \mathbb{E}_{X, X' \sim P} \left[\left(2\gamma + \frac{X^\top X' - \eta_{X' \rightarrow X}^\top X \eta_{X' \rightarrow X}^\top X'}{\sigma^4(d-1)} \right) {}_1F_1\left(\frac{1}{2}; \frac{d}{2}; -\gamma\|X - X'\|_2^2\right) \right] \\ &\quad + \mathbb{E}_{X, X' \sim P} \left[\frac{1}{d} \left(\frac{\eta_{X' \rightarrow X}^\top X \eta_{X' \rightarrow X}^\top X'}{\sigma^4} - \frac{X^\top X' - \eta_{X' \rightarrow X}^\top X \eta_{X' \rightarrow X}^\top X'}{\sigma^4(d-1)} \right) {}_1F_1\left(\frac{3}{2}; \frac{d}{2} + 1; -\gamma\|X - X'\|_2^2\right) \right] \\ &\quad + \mathbb{E}_{X, X' \sim P} \left[\frac{1}{d} \left(\frac{2\gamma}{\sigma^2} + 4\gamma^2 \right) \|X - X'\|_2^2 {}_1F_1\left(\frac{3}{2}; \frac{d}{2} + 1; -\gamma\|X - X'\|_2^2\right) \right]. \end{aligned}$$

[Source]

Proof Let $N \sim \mathcal{N}(0, \sigma^2 I_d)$. Note that for any $\xi \in \mathbb{S}^{d-1}$, we have $\text{law}(\xi^\top N) = \mathcal{N}(0, \sigma^2)$. By a direct calculation, it is simple to derive the following result,

$$\mathbb{K}_{\mathcal{N}(0, \sigma^2)} k_{\text{gsn}}(u, v) = \left[\frac{uv}{\sigma^4} - \left(\frac{2\gamma}{\sigma^2} + 4\gamma^2 \right) (u - v)^2 + 2\gamma \right] \exp(-\gamma(u - v)^2). \quad (29)$$

Recall that $d\mathcal{U}(\mathbb{S}^{d-1})(\xi) = \frac{\pi^{d/2}}{\Gamma(d/2)} d\xi =: C_d d\xi$. Now, the sliced KSD takes the following form,

$$\begin{aligned} \text{SKSD}^2(P, \mathcal{N}(0, \sigma^2 I_d)) &= C_d \mathbb{E}_{X, X' \sim P} \int_{\mathbb{S}^{d-1}} \left(\frac{\xi^\top X \xi^\top X'}{\sigma^4} + 2\gamma \right) \exp(-\gamma(\xi^\top(X - X'))^2) d\xi \\ &\quad - C_d \left(\frac{2\gamma}{\sigma^2} + 4\gamma^2 \right) \mathbb{E}_{X, X' \sim P} \int_{\mathbb{S}^{d-1}} (\xi^\top(X - X'))^2 \exp(-\gamma(\xi^\top(X - X'))^2) d\xi \quad (30) \\ &:= C_d \mathbb{E}_{X, X' \sim P} \left[\text{I}(X, X') + \left(\frac{2\gamma}{\sigma^2} + 4\gamma^2 \right) \text{II}(X, X') \right]. \end{aligned}$$

Recall the functions J_1, J_2 defined in Appendix App. G. Beginning with I, we have

$$I(x, x') = \underbrace{\int_{\mathbb{S}^{d-1}} \frac{\xi^\top x \xi^\top x'}{\sigma^4} \exp(-\gamma(\xi^\top(x-x'))^2) d\xi}_{I_1(x, x')} + 2\gamma J_1(\gamma\|x-x'\|_2^2).$$

Using the closed form expression for $I_1(x, x')$ derived in Lemma Thm. 13, we have

$$I(x, x') = \left(2\gamma + \frac{x^\top x' - e_1^\top x e_1^\top x'}{\sigma^4(d-1)}\right) J_1(\gamma\|x-x'\|_2^2) + \left(\frac{e_1^\top x e_1^\top x'}{\sigma^4} - \frac{x^\top x' - e_1^\top x e_1^\top x'}{\sigma^4(d-1)}\right) J_2(\gamma\|x-x'\|_2^2),$$

where $e_1 = \|x-x'\|_2^{-1}(x-x')$. Next, by Lemma Thm. 14, we have

$$\Pi(x, x') = \|x-x'\|_2^2 J_2(\gamma\|x-x'\|_2^2).$$

Putting these together, and substituting the closed forms for J_1, J_2 due to Lemmas Thm. 15 and Thm. 16, we have

$$\begin{aligned} & \text{SKSD}^2(P, \mathcal{N}(0, \sigma^2)) \\ &= C_d \mathbb{E}_{X, X' \sim P} \left[2 \frac{\pi^{d/2}}{\Gamma(d/2)} \left(2\gamma + \frac{X^\top X' - e_1^\top X e_1^\top X'}{\sigma^4(d-1)} \right) {}_1F_1\left(\frac{1}{2}; \frac{d}{2}; -\gamma\|X-X'\|_2^2\right) \right] \\ &+ C_d \mathbb{E}_{X, X' \sim P} \left[\frac{\pi^{d/2}}{\Gamma(d/2+1)} \left(\frac{e_1^\top X e_1^\top X'}{\sigma^4} - \frac{X^\top X' - e_1^\top X e_1^\top X'}{\sigma^4(d-1)} \right) {}_1F_1\left(\frac{3}{2}; \frac{d}{2} + 1; -\gamma\|X-X'\|_2^2\right) \right] \\ &+ C_d \mathbb{E}_{X, X' \sim P} \left[\frac{\pi^{d/2}}{\Gamma(d/2+1)} \left(\frac{2\gamma}{\sigma^2} + 4\gamma^2 \right) \|X-X'\|_2^2 {}_1F_1\left(\frac{3}{2}; \frac{d}{2} + 1; -\gamma\|X-X'\|_2^2\right) \right]. \end{aligned}$$

The claim follows by expanding C_d and simplifying, noting that

$$\frac{\Gamma(d/2)}{\Gamma(d/2+1)} = \frac{\Gamma(d/2)}{\frac{d}{2}\Gamma(d/2)} = \frac{2}{d}.$$

■

Lemma 13 *Let $x, x' \in \mathbb{R}^d$. Then define $I_1(x, x')$ via*

$$I_1(x, x') = \int_{\mathbb{S}^{d-1}} (\xi^\top x)(\xi^\top x') \exp(-\gamma(\xi^\top(x-x'))^2) d\xi.$$

It holds that

$$I_1(x, x') = (x^\top x' - (e_1^\top x)(e_1^\top x')) \frac{J_1(r\gamma^2) - J_2(r\gamma^2)}{d-1} + (e_1^\top x)(e_1^\top x') J_2(r\gamma^2),$$

where J_1, J_2 are defined in Appendix App. G.

Proof Let $\delta = x - x'$, and consider a coordinate system in which δ is parallel to the first basis vector denoted e_1 . Denoting by x_\perp the component of x orthogonal to e_1 , we have

$$\begin{aligned} \xi^\top x &= \xi_1(e_1^\top x) + \xi^\top x_\perp \\ \xi^\top x' &= \xi_1(e_1^\top x') + \xi^\top x'_\perp. \end{aligned}$$

Letting $r = \|x - x'\|_2$, we have

$$\begin{aligned} I_1(x, x') &= \underbrace{\int_{\mathbb{S}^{d-1}} \xi_1^2 (e_1^\top x)(e_1^\top x') \exp(-\gamma r^2 \xi_1^2) d\xi}_{f_1(x, x')} \\ &\quad + \int_{\mathbb{S}^{d-1}} \xi_1 (e_1^\top x)(\xi^\top x'_\perp) \exp(-\gamma r^2 \xi_1^2) d\xi \\ &\quad + \int_{\mathbb{S}^{d-1}} \xi_1 (e_1^\top x')(\xi^\top x_\perp) \exp(-\gamma r^2 \xi_1^2) d\xi \\ &\quad + \underbrace{\int_{\mathbb{S}^{d-1}} (\xi^\top x_\perp)(\xi^\top x'_\perp) \exp(-\gamma r^2 \xi_1^2) d\xi}_{f_2(x, x')}. \end{aligned}$$

Note that the integrands in the middle two terms are odd, so those integrals vanish. Moreover, we have

$$f_1(x, x') \equiv (e_1^\top x)(e_1^\top x') J_2(\gamma r^2).$$

Furthermore, by Lemma Thm. 17, we have

$$f_2(x, x') = x_\perp^\top x'_\perp \frac{J_1(\gamma r^2) - J_2(\gamma r^2)}{d-1}.$$

Altogether, we have shown that

$$I_1(x, x') = (x^\top x' - (e_1^\top x)(e_1^\top x')) \frac{J_1(\gamma r^2) - J_2(\gamma r^2)}{d-1} + (e_1^\top x)(e_1^\top x') J_2(\gamma r^2).$$

■

Lemma 14 *Let $x, x' \in \mathbb{R}^d$. Then it holds that*

$$\Pi(x, x') := \int_{\mathbb{S}^{d-1}} (\xi^\top (x - x'))^2 \exp(-\gamma (\xi^\top (x - x'))^2) d\xi = \|x - x'\|_2^2 \frac{\pi^{d/2}}{\Gamma(d/2 + 1)} {}_1F_1\left(\frac{3}{2}; \frac{d}{2} + 1; -\gamma \|x - x'\|_2^2\right).$$

Proof Let $\delta = x - x'$. Immediately, overloading notation, we have $\Pi(x, x') \equiv \Pi(\delta)$, where

$$\Pi(\delta) := \int_{\mathbb{S}^{d-1}} (\xi^\top \delta)^2 \exp(-\gamma (\xi^\top \delta)^2) d\xi.$$

Note that Π is rotationally symmetric. So, without loss of generality, we can take $\delta = r e_1$, where $r = \|\delta\|_2$ and e_1 is the first standard unit vector in \mathbb{R}^d . Then, we have

$$\begin{aligned} \Pi(\delta) &= \int_{\mathbb{S}^{d-1}} (r \xi_1)^2 \exp(-\gamma (r \xi_1)^2) d\xi \\ &= r^2 \int_{\mathbb{S}^{d-1}} \xi_1^2 \exp(-\gamma (r \xi_1)^2) d\xi. \end{aligned}$$

Now we've expressed Π as an integral of a function depending on only one coordinate over the unit sphere. Switching to polar coordinates, defining $\xi_1 = \cos \phi$, we have

$$\begin{aligned} \Pi(\delta) &= r^2 \text{Area}(\mathbb{S}^{d-2}) \int_0^\pi \cos^2 \phi \exp(-\gamma (r \cos \phi)^2) \sin^{d-2}(\phi) d\phi \\ &= r^2 \frac{2\pi^{(d-1)/2}}{\Gamma((d-1)/2)} \int_0^\pi \cos^2 \phi \exp(-\gamma (r \cos \phi)^2) \sin^{d-2}(\phi) d\phi. \end{aligned}$$

Now, writing $u := \xi_1$, we have $\sin^{d-2}(\phi) d\phi = -(1-u^2)^{(d-3)/2} du$, so that

$$\begin{aligned} \Pi(\delta) &= r^2 \frac{2\pi^{(d-1)/2}}{\Gamma((d-1)/2)} \int_{-1}^1 u^2 (1-u^2)^{(d-3)/2} \exp(-\gamma r^2 u^2) du \\ &= 2r^2 \frac{2\pi^{(d-1)/2}}{\Gamma((d-1)/2)} \int_0^1 u^2 (1-u^2)^{(d-3)/2} \exp(-\gamma r^2 u^2) du. \end{aligned}$$

We will now express this in terms of ${}_1F_1$. Recall that

$${}_1F_1(a; b; z) = \frac{\Gamma(b)}{\Gamma(a)\Gamma(b-a)} \int_0^1 t^{a-1}(1-t)^{b-a-1} e^{zt} dt.$$

To relate $\Pi(\delta)$ to ${}_1F_1$, we write $t := u^2$, so that $du = \frac{1}{2}t^{-1/2}dt$, yielding

$$\Pi(\delta) = r^2 \frac{2\pi^{(d-1)/2}}{\Gamma((d-1)/2)} \int_0^1 t^{1/2}(1-t)^{(d-3)/2} \exp(-\gamma r^2 t) dt.$$

Now let $a = 3/2$, $b = d/2 + 1$, and $z = -\gamma r^2$, so that

$$\begin{aligned} \Pi(\delta) &= r^2 \frac{2\pi^{(d-1)/2}}{\Gamma((d-1)/2)} \int_0^1 t^{a-1}(1-t)^{b-a-1} \exp(zt) dt \\ &= r^2 \frac{2\pi^{(d-1)/2}}{\Gamma((d-1)/2)} \left[\left(\frac{\Gamma(d/2+1)}{\Gamma(3/2)\Gamma((d-3)/2)} \right)^{-1} {}_1F_1\left(\frac{3}{2}; \frac{d}{2} + 1; z\right) \right] \\ &= \|x - x'\|_2^2 \frac{\pi^{d/2}}{\Gamma(d/2+1)} {}_1F_1\left(\frac{3}{2}; \frac{d}{2} + 1; -\gamma \|x - x'\|_2^2\right). \end{aligned}$$

■

G Hypergeometric Integrals

In this section, we compute various integrals that will be useful throughout the text. Henceforth, we fix $u, v \in \mathbb{R}^d$ and $\gamma > 0$, and we define the following integrals:

$$J_1(c) := \int_{\mathbb{S}^{d-1}} \exp(-c\xi_1^2) d\xi, \quad c \in \mathbb{R}. \quad (31)$$

$$J_2(c) := \int_{\mathbb{S}^{d-1}} \xi_1^2 \exp(-c\xi_1^2) d\xi, \quad c \in \mathbb{R}. \quad (32)$$

Lemma 15 *We have that*

$$J_1(c) = \frac{2\pi^{d/2}}{\Gamma(d/2)} {}_1F_1\left(\frac{1}{2}; \frac{d}{2}; -c\right).$$

Proof This is the well-known closed form of the Gaussian integral on the sphere. ■

Lemma 16 *We have that*

$$J_2(c) = \frac{\pi^{d/2}}{\Gamma(d/2+1)} {}_1F_1\left(\frac{3}{2}; \frac{d}{2} + 1; -c\right).$$

Proof This follows directly from Lemma Thm. 14. ■

Lemma 17 *Suppose u, v are orthogonal to e_1 , the first unit basis vector. Then*

$$\int_{\mathbb{S}^{d-1}} (\xi^\top u)(\xi^\top v) \exp(-c\xi_1^2) d\xi = (u^\top v) \frac{J_1(c) - J_2(c)}{d-1}.$$

Proof Firstly, note that for $i, j \neq 1$ and $i \neq j$, we have

$$\int_{\mathbb{S}^{d-1}} \xi_i \xi_j \exp(-c\xi_1^2) d\xi = 0$$

since the integrand is odd. Moreover, by symmetry, it is clear that

$$\int_{\mathbb{S}^{d-1}} \xi_i^2 \exp(-c\xi_1^2) d\xi = \int_{\mathbb{S}^{d-1}} \xi_j^2 \exp(-c\xi_1^2) d\xi$$

for any $i, j \geq 2$. Since for any $\xi \in \mathbb{S}^{d-1}$ we have by definition $\sum_{i=1}^d \xi_i^2 = 1$, we have

$$\begin{aligned} J_1(c) &= \sum_{i=1}^d \int_{\mathbb{S}^{d-1}} \xi_i^2 \exp(-c\xi_1^2) d\xi \\ &= J_2(c) + (d-1) \int_{\mathbb{S}^{d-1}} \xi_i^2 \exp(-c\xi_1^2) d\xi \quad i \geq 2 \\ \therefore \int_{\mathbb{S}^{d-1}} \xi_i^2 \exp(-c\xi_1^2) d\xi &= \frac{J_1(c) - J_2(c)}{d-1}. \end{aligned}$$

We can now relate this result to the integral we wish to compute. Particularly, we have

$$\begin{aligned} \int_{\mathbb{S}^{d-1}} (\xi^\top u)(\xi^\top v) \exp(-c\xi_1^2) d\xi &= \sum_{i=2}^d \sum_{j=2}^d \int_{\mathbb{S}^{d-1}} u_i v_j \xi_i \xi_j \exp(-c\xi_1^2) d\xi \\ &= \sum_{i=2}^d u_i v_i \int_{\mathbb{S}^{d-1}} \xi_i^2 \exp(-c\xi_1^2) d\xi \\ &= u^\top v \frac{J_1(c) - J_2(c)}{d-1}. \end{aligned}$$

■

H Learning with Hyperspherical Representations

Many self-supervised learning algorithms leverage normalization of representations onto the unit hypersphere \mathbb{S}^{d-1} . We demonstrate that the DIPReg framework is geometry-agnostic: by selecting the appropriate manifold (hypersphere) and prior (uniform), we recover and extend known regularization techniques.

We utilize the rotationally invariant *von Mises–Fisher* (vMF) kernel, defined for $x, y \in \mathbb{S}^{d-1}$ and concentration $\kappa > 0$ as:

$$k_{\text{vMF}}(x, y) = \exp(\kappa x^\top y). \quad (33)$$

H.1 Maximum Mean Discrepancy with Uniform Prior

We first show that applying the standard MMD estimator with a vMF kernel and a Uniform prior recovers the pairwise hyperspherical energy objective.

Proposition 18 *Let P be a distribution on \mathbb{S}^{d-1} and \mathcal{U} be the uniform distribution on \mathbb{S}^{d-1} . The squared MMD with kernel k_{vMF} is given up to an additive constant by:*

$$\text{MMD}_{\text{vMF}}^2(P, \mathcal{U}) = \mathbb{E}_{X, X' \sim P}[\exp(\kappa X^\top X')] + C_{\kappa, d}, \quad (34)$$

where $C_{\kappa, d}$ is a constant independent of P .

Proof Recall the definition of the squared MMD:

$$\text{MMD}_{\text{vMF}}^2(P, \mathcal{U}) = \mathbb{E}_{X, X' \sim P}[k(X, X')] - 2\mathbb{E}_{X \sim P, Y \sim \mathcal{U}}[k(X, Y)] + \mathbb{E}_{Y, Y' \sim \mathcal{U}}[k(Y, Y')].$$

The third term is clearly constant with respect to P . We analyze the second term (the cross-term). Due to the rotational invariance of the Uniform measure and the kernel, the inner expectation is independent of x . Specifically, for any fixed $x \in \mathbb{S}^{d-1}$:

$$\mathbb{E}_{Y \sim \mathcal{U}}[\exp(\kappa x^\top Y)] = \int_{\mathbb{S}^{d-1}} \exp(\kappa x^\top y) d\mathcal{U}(y) = (2\pi)^{d/2} \kappa^{-(d/2-1)} I_{d/2-1}(\kappa),$$

where I_ν is the modified Bessel function of the first kind. Since this value is independent of x , the entire term $-2\mathbb{E}_{X, Y}[k(X, Y)]$ collapses into the constant $C_{\kappa, d}$. The only term dependent on P is the first term, which corresponds to the pairwise potential energy. ■

H.2 Kernel Stein Discrepancy as a Uniformity Regularizer

We now derive the Kernel Stein Discrepancy for the Uniform distribution on the sphere. Unlike MMD, this allows for regularization using the intrinsic geometry of the manifold without requiring Bessel function evaluations or sampling from the prior.

Proposition 19 *Let \mathcal{U} be the uniform distribution on \mathbb{S}^{d-1} . The Stein kernel k_{stein} associated with k_{vMF} and target \mathcal{U} is given by:*

$$k_{\text{stein}}(x, y) = \kappa \exp(\kappa(x^\top y)) [\kappa(x^\top y)^3 + (x^\top y)^2 - \kappa(x^\top y) + d - 2]. \quad (35)$$

Proof The score function of the uniform distribution vanishes on the manifold, i.e., $s_{\mathcal{U}}(x) = \nabla_{\mathbb{S}} \log p_{\mathcal{U}}(x) = 0$. Consequently, the Stein kernel reduces to the trace of the Riemannian Hessian of the base kernel:

$$k_{\text{stein}}(x, y) = \text{tr}(\nabla_{\mathbb{S}, y} \nabla_{\mathbb{S}, x} k_{\text{vMF}}(x, y)).$$

Let $t = x^\top y$. The Euclidean gradient of the kernel with respect to x is $\nabla_x \exp(\kappa t) = \kappa y \exp(\kappa t)$. The Riemannian gradient is the projection of this vector onto the tangent space $T_x \mathbb{S}^{d-1}$ using the projector $P_x = (I - xx^\top)$:

$$\nabla_{\mathbb{S}, x} k = P_x(\kappa y \exp(\kappa t)) = \kappa \exp(\kappa t)(y - tx).$$

To compute the Stein kernel, we require the divergence of this vector field with respect to y . We utilize the identity $\text{div}_{\mathbb{S}}(V) = \text{tr}(P_y \nabla_y V)$, where ∇_y denotes the Euclidean Jacobian. Let $V(y) := \kappa \exp(\kappa t)(y - tx)$. We compute the Euclidean Jacobian $M = \nabla_y V$:

$$M = \nabla_y [\kappa \exp(\kappa t)(y - tx)] = \kappa [(\nabla_y \exp(\kappa t))(y - tx)^\top + \exp(\kappa t) \nabla_y (y - tx)].$$

Noting that $\nabla_y t = x$, we have:

$$M = \kappa^2 \exp(\kappa t) x (y - tx)^\top + \kappa \exp(\kappa t) (I - xx^\top).$$

We now compute the trace of the projected Jacobian, $\text{tr}(P_y M) = \text{tr}((I - yy^\top)M) = \text{tr}(M) - y^\top M y$.

First, the trace of M :

$$\text{tr}(M) = \kappa^2 \exp(\kappa t) (y - tx)^\top x + \kappa \exp(\kappa t) \text{tr}(I - xx^\top) = \kappa(d - 1) \exp(\kappa t).$$

Second, the quadratic contraction $y^\top M y$:

$$\begin{aligned} y^\top M y &= \kappa^2 \exp(\kappa t) (y^\top x) (y - tx)^\top y + \kappa \exp(\kappa t) y^\top (I - xx^\top) y \\ &= \kappa^2 t \exp(\kappa t) (1 - t^2) + \kappa \exp(\kappa t) (1 - t^2). \end{aligned}$$

Subtracting the terms yields the result:

$$\begin{aligned} k_{\text{stein}}(x, y) &= \kappa(d - 1) \exp(\kappa t) - \exp(\kappa t) (1 - t^2) (\kappa^2 t + \kappa) \\ &= \kappa \exp(\kappa t) [(d - 1) - (1 - t^2)(\kappa t + 1)]. \end{aligned}$$

Rearranging the polynomial terms in t completes the proof. ■

I Extended Results

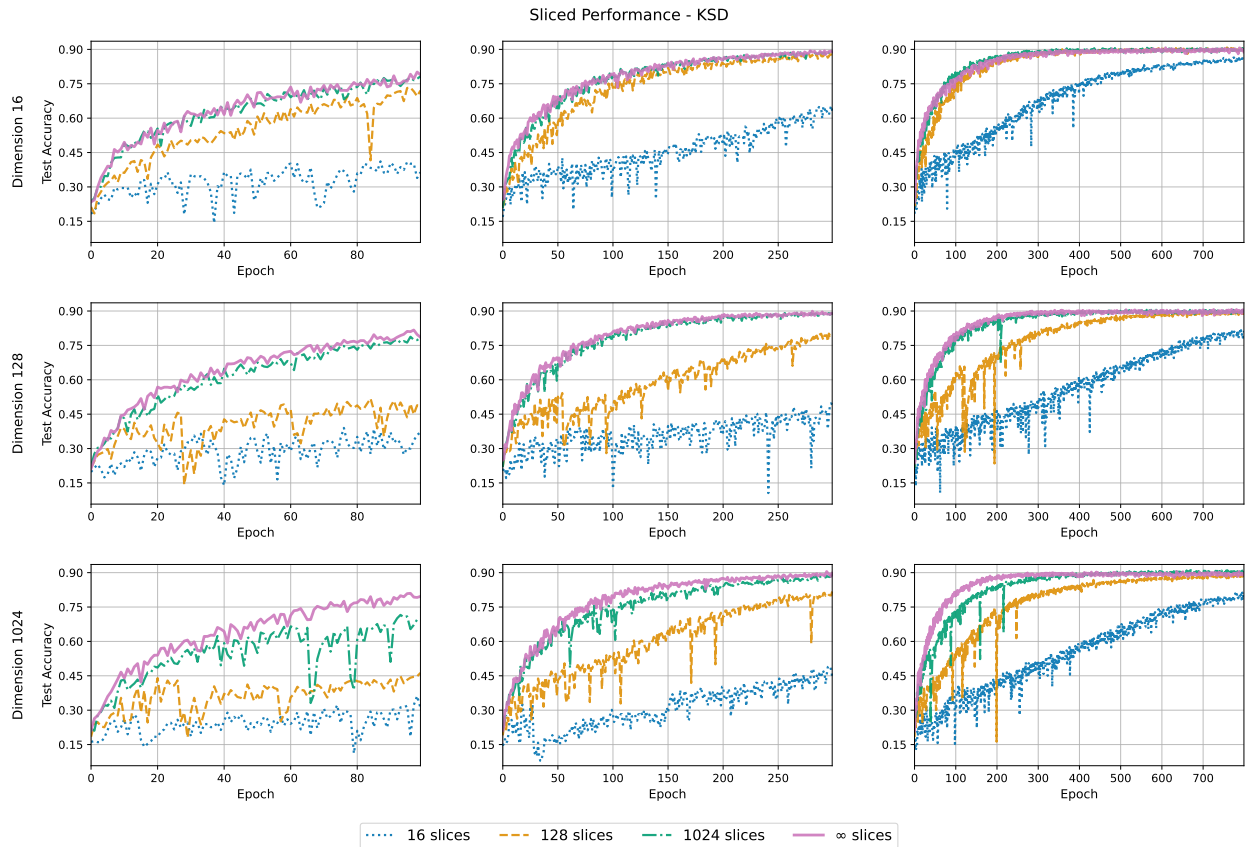


Figure 3: Impacts of slicing in various dimensions for the KSD regularizer on ImageNette, measuring test accuracy over various training horizons. Results indicate that insufficient slices slow convergence rates as a function of dimension and introduces instability in the early half of training compared to the analytically sliced counterpart.